ACCSCIENCE PUBLISHING

International Journal of Bioprinting

REVIEW ARTICLE

Multiscale 3D printing for hierarchical reconstruction and functional regeneration of bone tissue

Yueyang Wang[1†], Yazhe Fan[1†], Yue Wang[2], Maisha Feng[2], Li Ji[3], Jinfan Wei[1], Linyi Wang[1], Lin Zhu[4*], Yujie Wang[2*], and Pengbei Fan[5,6*]

[1]School of Bone and Joint Medicine, Henan University of Chinese Medicine, Zhengzhou, Henan, China

[2]School of Traditional Chinese Medicine, Henan University of Chinese Medicine, Zhengzhou, Henan, China

[3]The Third Clinical Medical College of Henan University of Chinese Medicine, Zhengzhou, Henan, China

[4]Department of Orthopedics, The Third Affiliated Hospital of Henan University of Chinese Medicine, Zhengzhou, Henan, China

[5]School of Traditional Chinese Medicine, Southern Medical University, Guangzhou, Guangdong, China

[6]Wangqi Academy of Beijing University of Chinese Medicine, National Institute of TCM Constitution and Preventive Treatment of Disease, Beijing University of Chinese Medicine, Beijing, China

[†]*These authors contributed equally to this work.*

***Corresponding authors:**
Lin Zhu
(2325221990@qq.com);
Yujie Wang
(wyj00218@126.com);
Pengbei Fan
(dc_fpb@163.com)

Citation: Wang Y, Fan Y, Wang Y, *et al*. Multiscale 3D printing for hierarchical reconstruction and functional regeneration of bone tissue. *Int J Bioprint*. 2026;12(5):026280296. doi: 10.36922/IJB026280296

Received: July 8, 2026

Revised: July 29, 2026

Accepted: August 5, 2026

Published online: August 6, 2026

Copyright: © 2026 Author(s). This is an Open-Access article distributed under the terms of the Creative Commons Attribution License, permitting distribution, and reproduction in any medium, provided the original work is properly cited.

Publisher's Note: AccScience Publishing remains neutral with regard to jurisdictional claims in published maps and institutional affiliations.

Abstract

Bone tissue engineering (BTE) has emerged as a promising approach for repairing critical bone defects that remain challenging to treat using conventional grafting strategies. Recent advances in three-dimensional (3D) printing have enabled the fabrication of patient-specific and biomimetic bone constructs with precise control over structural architecture, material composition, and biological functionality. However, native bone exhibits a highly hierarchical organization spanning multiple length scales, and current 3D printing approaches often remain limited by insufficient integration between macroscopic mechanical reconstruction, microscale cellular regulation, and nanoscale bioactive signaling. In this review, we provide a comprehensive overview of multiscale 3D printing strategies for bone tissue reconstruction, highlighting how additive manufacturing technologies facilitate the recapitulation of hierarchical bone structures. We first summarize the historical evolution of 3D printing in BTE and discuss advances in bioinks, biomaterials, and printing technologies. Subsequently, we analyze multiscale reconstruction strategies from three perspectives: macroscale fabrication for personalized anatomical restoration and mechanical support, microscale construction for cellular organization and vascular network formation, and nanoscale engineering for biomimetic extracellular matrix interfaces and molecular regulation. Furthermore, we discuss emerging strategies integrating smart responsive materials, bioactive cues, and computational design to enhance the regenerative capacity of 3D-printed bone constructs. Finally, current challenges and future perspectives are presented, focusing on vascularization, immune regulation, artificial intelligence-assisted scaffold optimization, four-dimensional bioprinting, and clinical translation. This review highlights the potential of multiscale 3D printing as a transformative platform for developing functional bone tissues and advancing personalized regenerative medicine.

Keywords: Multiscale 3D bioprinting; Bone tissue engineering; Biofabrication; Tissue reconstitution; Regenerative medicine

1. Introduction

Bone tissue, as a vital component of the human body, performs multiple essential physiological functions, including providing structural support, protecting vital organs, participating in metabolism, and supporting hematopoiesis.[1] However, bone defects have increasingly become one of the most complex and challenging pathological problems in orthopedic practice.[2] Bone tissue damage can be caused by a variety of factors, including trauma, infection, tumor resection, congenital malformations, and degenerative diseases (Figure 1A). Fracture healing is a highly complex and precisely regulated biological process that requires coordinated control of multiple stages, including inflammation, angiogenesis, endochondral ossification, and intramembranous ossification.[3,4] This process relies on the dynamic balance and fine regulation of various cell types (such as osteoblasts, osteoclasts, and fibroblasts), the extracellular matrix (ECM), and signaling molecules.[5] When the size of a bone defect exceeds the critical threshold, the intrinsic regenerative capacity of the body is markedly limited, necessitating exogenous interventions to promote bone regeneration and functional reconstruction.[6] It has been reported that approximately two million bone grafting or bone reconstruction procedures are performed worldwide each year.[7] For patients with large segmental bone defects, the outcomes of existing repair strategies remain suboptimal, with clinically reported healing success rates of only about 80%.[8] Bone defects are characterized by a high incidence and significant difficulty in repair, highlighting the clear limitations of current therapeutic approaches.

Currently, the primary clinical approaches for treating bone defects include autologous bone grafting, allogeneic bone grafting, and synthetic bone substitutes (Figure 1B). Autologous bone grafts remain the clinical benchmark because they provide viable osteogenic cells, an osteoconductive matrix, and endogenous osteoinductive cues.[9] However, their use is limited by the restricted availability of donor bone and the need for an additional harvesting procedure, which increases surgical trauma, blood loss, and the risk of donor-site complications such as pain, fracture, and infection.[10] Allogeneic bone grafts partially address donor shortages but generally lack viable osteogenic cells and may exhibit reduced osteoinductive activity, although they can retain an osteoconductive matrix; risks of immune rejection and disease transmission also remain. To address the shortcomings of biological grafts, various synthetic bone substitutes, including ceramics, metals, and polymers, have been developed. Due to their abundant availability, controllable composition, and favorable biosafety, synthetic grafts have become an important alternative for bone repair. Nevertheless, most existing synthetic materials provide mainly structural support while lacking adequate osteoinductive activity, and their degradation rates are often mismatched with natural bone regeneration, leading to suboptimal mechanical and biological outcomes.[11] Consequently, the development of more personalized, functional, and regenerative strategies, particularly tissue engineering approaches that integrate bioactive regulation with multiscale biomimetic design, has emerged as a key direction for advancing bone repair (Figure 1C).

In recent years, with the rapid advancement of tissue engineering and regenerative medicine, three-dimensional (3D) printing has demonstrated significant potential in bone tissue repair.[12,13] Based on 3D digital models, 3D printing enables the layer-by-layer fabrication of complex architectures with precise control over both macroscopic geometry and microscopic structure for personalized bone defect reconstruction.[14] Patient-specific scaffolds can be directly generated from medical imaging data, such as computed tomography (CT) or magnetic resonance imaging, to accurately match the defect site in terms of shape, size, and internal porosity.[15] More importantly, 3D printing has evolved from a manufacturing technique into a versatile platform for multiscale biomimetic scaffold construction. By precisely tuning printing parameters, including layer thickness, printing paths, pore size distribution, and material composition, it is possible to recapitulate the hierarchical structural features of native bone, ranging from macroscopic mechanical support to microscale porous networks and even nanoscale interfacial regulation (Figure 2A). Such scaffold designs provide sufficient mechanical strength to withstand physiological loads while creating an optimal 3D microenvironment for cell adhesion, migration, and angiogenesis.[16,17] Furthermore, 3D printing enables the integration of diverse functional biomaterials, including bioceramics (e.g., hydroxyapatite [HA] and beta-tricalcium phosphate [β-TCP]), biodegradable polymers (e.g., poly(lactic-co-glycolic acid) [PLGA] and polycaprolactone [PCL]), and metal alloys (e.g., titanium and magnesium). The use of bio-inks also allows the incorporation of osteogenic cells,

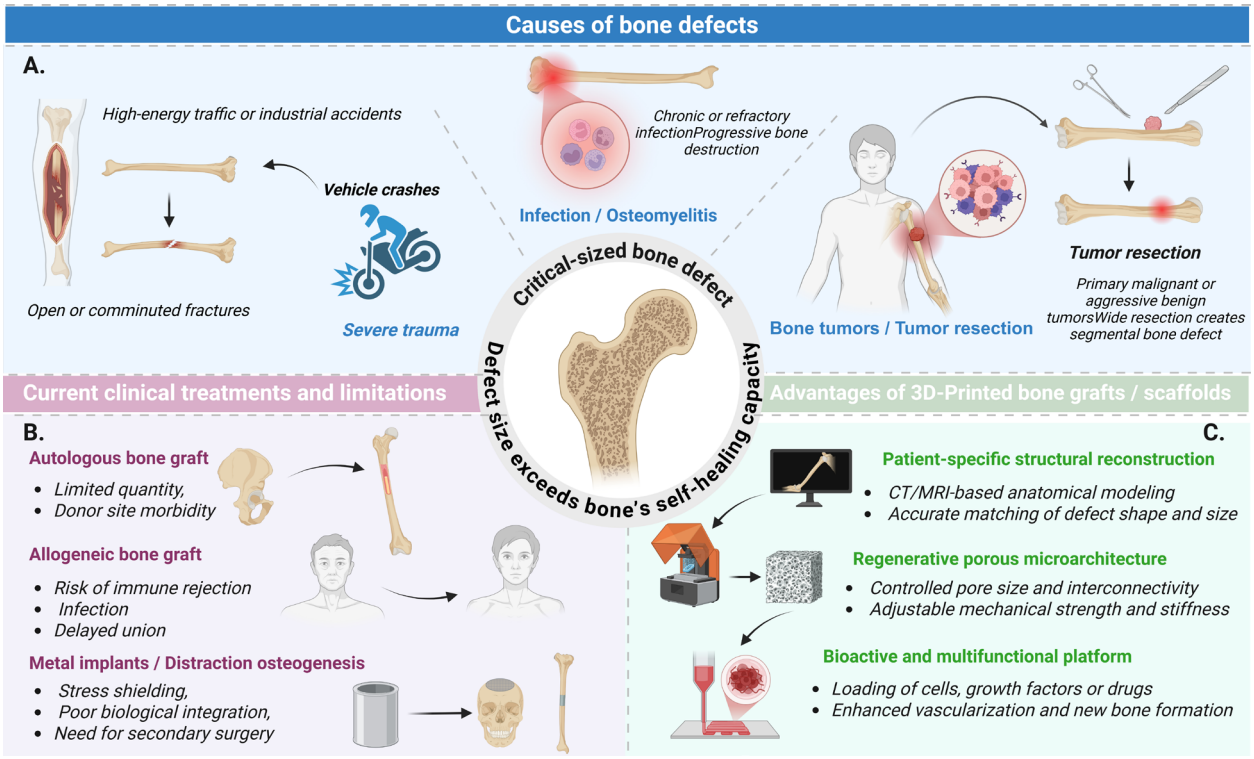


Figure 1. Etiology of critical-sized bone defects, limitations of current treatments, and advantages of 3D-printed scaffolds. (A) Three principal causes of critical-sized bone defects: severe trauma, infection/osteomyelitis, and tumor resection. (B) Key limitations of existing clinical strategies, including donor-site morbidity (autografts), immune rejection (allografts), and stress shielding requiring revision surgery (metal implants). (C) Core advantages of 3D-printed bone scaffolds: patient-specific anatomical reconstruction, tunable porous microarchitecture, and a bioactive platform for loading cells, growth factors, or drugs to promote bone regeneration. Created in BioRender. Yang, W. (2026). https://BioRender.com/tyty4eo.
Abbreviations: 3D: Three-dimensional; CT: Computed tomography; MRI: Magnetic resonance imaging.

growth factors, and ECM components, thereby further enhancing the bioactivity and regenerative potential of the constructs. Owing to its unique advantages in structural precision and functional integration, 3D printing is increasingly recognized as a central strategy in bone tissue engineering (BTE).

To ensure conceptual consistency, the terminology and scale classifications used in this review are defined according to both fabrication processes and the hierarchical organization of bone. "3D printing" and "additive manufacturing" are used as general terms for layer-by-layer fabrication technologies, including acellular approaches such as fused deposition modeling (FDM), selective laser sintering (SLS), selective laser melting (SLM), and electron beam melting (EBM), whereas "3D bioprinting" refers specifically to the spatially controlled deposition of living cells or cell-laden bioinks under cytocompatible conditions. Accordingly, metallic, ceramic, and thermoplastic constructs fabricated without living components are described as 3D-printed or additively manufactured scaffolds, while the term "bioprinting" is reserved for fabrication processes that directly involve cells or bioinks. In parallel, the macro-, micro-, and nanoscale categories discussed throughout this review are defined primarily by their structural and functional roles rather than by rigid dimensional thresholds. The macroscale relates mainly to anatomical geometry, overall scaffold architecture, and bulk mechanical performance; the microscale encompasses pores, fibers, channels, cellular organization, and local transport environments; and the nanoscale includes surface topography, nanofibrous features, nanoparticles, protein–material interfaces, and molecular signaling cues. Notably, most nanoscale strategies in BTE rely on nanoscale material or interfacial engineering integrated with conventionally printed constructs, rather than direct fabrication of entire scaffolds at nanometer resolution. This framework provides the conceptual basis for understanding how fabrication methods and design features across multiple scales can be coordinated to support anatomical reconstruction, mechanical competence, vascularization, and biologically instructive cell–material interactions.

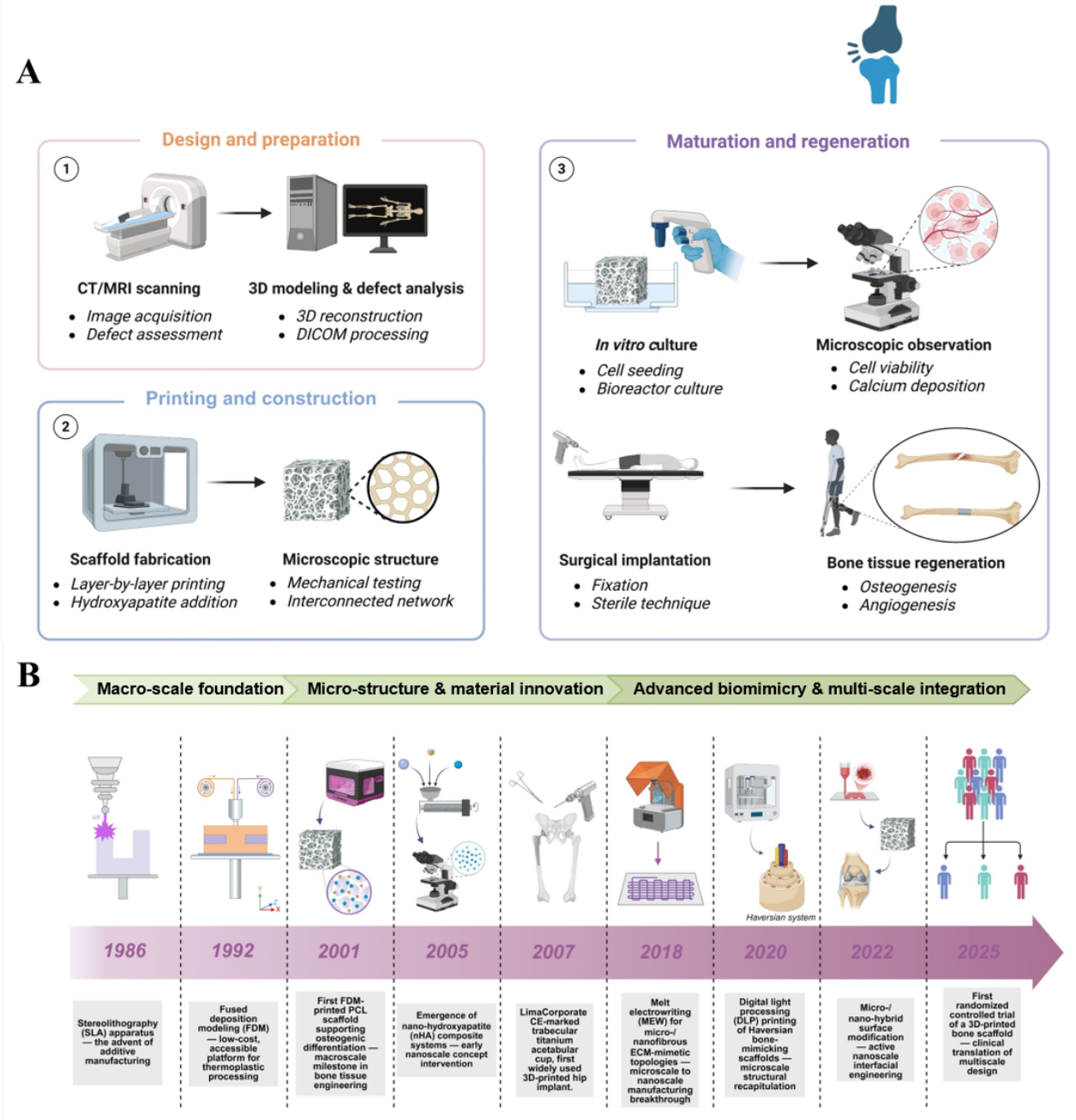


Figure 2. Evolution and workflow of 3D printing technologies for bone tissue engineering. (A) General workflow of 3D printing-assisted bone defect repair, including medical imaging acquisition, digital modeling, scaffold fabrication, biological evaluation, implantation, and tissue regeneration. (B) Historical evolution of 3D printing technologies in bone tissue engineering, highlighting the transition from macroscopic structural fabrication toward microscale organization, biofunctional integration, and multiscale regenerative strategies. Created in BioRender. Yang, W. (2026). https://BioRender.com/tyty4eo.

Abbreviations: 3D: Three-dimensional; CT: Computed tomography; DICOM: Digital Imaging and Communications in Medicine; MRI: Magnetic resonance imaging.

In this review, we first outline the historical development of 3D printing in BTE, followed by a scale-based discussion of bioink design, printing strategies, and applications in bone reconstruction. The review is systematically organized to summarize 3D printing applications across multiple scales—from macroscale scaffold fabrication to micro- and nanoscale biofabrication—emphasizing how multiscale bioprinting strategies facilitate the recapitulation of

bone's hierarchical structure and promote effective tissue regeneration.

2. Applications of 3D printing in bone tissue reconstruction

2.1. The historical evolution of 3D printing in bone tissue engineering

The application of 3D printing in BTE has undergone an interdisciplinary transition from industrial manufacturing to biomedicine (Figure 2B). Over nearly four decades, the progressive refinement of multiscale fabrication capabilities has been the central theme.

2.1.1. Foundation period of macroscale fabrication (1980s–1990s)

In 1986, Charles W. Hull was granted a United States patent for stereolithography (SLA), marking a major milestone in the development of additive manufacturing.[18] Subsequently, key technologies including SLS (1987),[19] FDM (1992),[20] and 3D printing (1994) emerged.[21] These breakthroughs primarily addressed the precise fabrication of macroscale 3D structures, laying the manufacturing foundation for future biomedical applications.

2.1.2. Emergence of microscale structure control (2000s)

In 2001, Hutmacher *et al.*[22] successfully fabricated biodegradable PCL scaffolds using FDM, demonstrating that synthetic polymers could be reliably printed into porous microscale structures supporting cell adhesion, proliferation, and osteogenic differentiation. This milestone shifted the focus from "can it be printed?" to "how can microscale structures regulate regenerative function?", paving the way for multi-material scaffold design and translational applications.

2.1.3. Expansion toward multiscale biofabrication (2010s–2020s)

Recent advances in bioprinting have driven the field from acellular scaffolds toward cell-laden, dynamic, and multifunctional multiscale bone constructs. The hallmark is multiscale integration: macroscale matching of defect geometry, microscale construction of cellular and vascular networks, and nanoscale modulation of cellular behavior via bioactive ions and signaling molecules. In 2019, Anada *et al.*[23] reported a biomimetic hydrogel 3D printing system that promoted osteogenic and angiogenic gene expression *in vitro*, demonstrating the feasibility of microscale osteo-vascular coupling. In 2020, Chiesa *et al.*[24] established a vascularized bone model using a co-culture system, achieving capillary neogenesis and spatiotemporal coordination of bone–vascular networks within 3D-printed constructs. In 2022, Shen *et al.*[25] fabricated vascularized tissue-engineered bone via 3D bioprinting and confirmed its excellent regenerative performance in a rat critical-sized cranial defect model, with histology showing enhanced new bone formation and rapid host vascular ingrowth. Gong *et al.*[26] reported a prospective multicenter randomized controlled trial of the Bongolle® scaffold, providing early clinical evidence regarding its safety and efficacy in the repair of critical-sized bone defects. Overall, the development of 3D printing in BTE represents a continuous deepening of multiscale fabrication capabilities—from precise macroscale structuring, through fine microscale pore regulation, to spatial coordination of cell–vascular networks, and finally nanoscale integration of signaling molecules. This evolutionary trajectory illustrates the progression of multiscale 3D printing from "structural biomimicry" toward "functional regeneration," providing a historical rationale for the multiscale printing strategies discussed in this review.

2.2. Materials and bioinks for 3D printing in bone tissue engineering

In 3D printing-based BTE, printing materials and bioinks serve not only as structural components of scaffolds but also as platforms for cell delivery and biochemical and mechanical regulation. Scaffold materials should exhibit appropriate biocompatibility, mechanical properties, degradation behavior, and processibility.[27] Specifically, the materials and their degradation products should be non-toxic and non-immunogenic; the ink should possess suitable rheological properties and structural stability to provide adequate mechanical support; it must allow precise and reproducible fabrication under specific printing modalities (e.g., extrusion, photopolymerization, or inkjet printing); and it should support cell adhesion, proliferation, and osteogenic differentiation while gradually degrading *in vivo* to be replaced by newly formed bone. Given the hierarchical complexity of bone, rational material selection and bioink design are crucial for integrating structural integrity and biological functionality in 3D-printed bone constructs (Table 1; Figure 3).

2.2.1. Bioceramics

Bioceramics, among the earliest materials used for bone repair, are widely applied in 3D-printed bone scaffolds due to their chemical similarity to the inorganic mineral phase of natural bone, excellent biocompatibility, and osteoconductivity. Based on chemical properties and biocompatibility, bioceramics can be classified into bioinert and bioactive ceramics. Bioinert ceramics, represented by zirconia (ZrO_2), exhibit chemical stability and good

Table 1. Comparison of representative biomaterials and bioinks used in 3D printing and bioprinting for bone tissue engineering

Material category	Representative materials	Degradability	Bone-regenerative activity	Key advantages	Main limitations	Application scope	References
Bioceramics							
Bioinert ceramics	Zirconia	Non-degradable	None (bioinert)	High fracture toughness; high-precision dental restorations can be fabricated via digital light processing 3D printing (flexural strength 940 MPa, fracture toughness 6.92 MPa·$m^{1/2}$); excellent chemical stability, corrosion and wear resistance; reduced bacterial adhesion.	Bioinert with no proactive osteogenic capacity; stress shielding effect; osseointegration relies on mechanical interlocking without chemical bonding; brittleness limits application under non-axial loading.	Dental restoration; joint load-bearing sites	28-30
Bioactive ceramics (calcium phosphates)	HA; β-TCP; BCP	(i) HA: Extremely slow (years) (ii) β-TCP: Moderate (months–years) (iii) BCP: Tunable (via HA/β-TCP ratio)	Excellent osteoconductivity (driven by Ca^{2+}/PO_4^{3-} chemistry)	Highly similar composition to the inorganic mineral phase of native bone; excellent osteoconductivity of HA; BCP enables on-demand balance of stability and degradation rate by adjusting the HA/β-TCP ratio.	Extremely slow degradation of HA (years), hindering bone tissue replacement; low strength of β-TCP (only suitable for non-load-bearing sites); high brittleness and poor toughness.	Non-load-bearing bone defects; cancellous bone filling	31-33
Bioactive ceramics (silicates)	Akermanite ($Ca_2MgSi_2O_7$); $CaSiO_3$	Degradable (moderate rate)	Strong (synergistic effect of Ca^{2+}/Mg^{2+}/Si^{4+} ions)	Synergistic osteogenesis driven by multiple ions including Ca^{2+}, Mg^{2+} and Si^{4+}; Mg^{2+} enhances mineralization, Si^{4+} promotes angiogenesis; promotes bone repair by activating osteogenesis-related signaling pathways.	Risk of ion burst release in the initial degradation stage; insufficient long-term degradation matching; insufficient large-animal and long-term clinical evidence.	Non-load-bearing bone defects; coating materials	34-36
Metallic materials							
Titanium alloy (Ti–6Al–4V)	Ti–6Al–4V (fabricated via SLM/EBM)	Non-degradable	Weak (surface modification required)	High fatigue strength and corrosion resistance; patient-specific porous lattice architecture can be constructed via SLM/EBM; widely applied in clinical practice.	Elastic modulus far exceeds that of bone tissue, causing significant stress shielding effect and periprosthetic bone loss; surface bioinertness; long-term stability of HA coating to be verified.	Load-bearing bone defects; complex bone reconstruction	29,37-39

(*cont'd...*)

Table 1. (*Continued*)

Material category	Representative materials	Degradability	Bone-regenerative activity	Key advantages	Main limitations	Application scope	References
Magnesium-based alloys	WE43; Mg–Ca; Mg–Zn	Degradable (relatively fast corrosion rate)	Strong: Mg^{2+} regulates immune microenvironment, activates osteogenic signaling, promotes vascularization, and inhibits osteoclasts	Elastic modulus close to native bone (41–45 GPa), eliminating stress shielding; actively promotes bone regeneration; degradable to avoid secondary surgery; Mg^{2+} is an essential ion with high biocompatibility.	Relatively fast corrosion rate; hydrogen evolution reaction may cause subcutaneous emphysema; mechanical integrity is lost before bone healing is completed.	Non-load-bearing or short-term load-bearing sites	40-43
Zinc-based alloys	Pure Zn; Zn–Li; Zn–Y; LPBF-fabricated Zn	Degradable (generally more moderate than Mg; composition- and structure-dependent)	Osteogenic and angiogenic potential through controlled Zn^{2+} release; dose- and composition-dependent	Moderate degradation kinetics without hydrogen evolution; Zn^{2+} participates in bone metabolism; LPBF enables patient-specific porous structures and microstructural regulation.	Limited strength of pure Zn; high vapor pressure may cause evaporation and porosity during LPBF; process-induced anisotropy; excessive Zn^{2+} release may impair cytocompatibility; limited long-term and clinical evidence.	Biodegradable bone scaffolds; small bone fixation devices; guided bone regeneration membranes; orthopedic implants under preclinical evaluation	44-47
Tantalum	Porous pure tantalum (fabricated via SLM)	Non-degradable	Osteoconductive; promotes osseointegration	Excellent corrosion resistance; highly porous interconnected architecture can facilitate bone ingrowth; high long-term survival rate of clinical implants.	High density (16.6 g/cm^3) and high melting point (2,996 °C) lead to extremely high processing cost; decreased fatigue strength of high-porosity scaffolds; clinical translation pathways remain uncertain.	Joint replacement; spinal fusion; osteonecrosis of the femoral head	48-50
Polymers							
Natural polymers	Gelatin/GelMA Alginate; Chitosan; Silk fibroin	Degradable (wide variation among materials)	Strong (RGD sequence mimicking native ECM)	Contains cell recognition sites (RGD sequence), highly similar to native ECM; supports cell adhesion, proliferation, and osteogenic differentiation; alginate/bacterial cellulose/PCL composite compressive modulus matches that of cancellous bone (31–48 MPa).	Insufficient mechanical strength, unsuitable for load-bearing sites; difficult to precisely regulate the degradation rate; contradiction between printing accuracy and cell viability for some materials.	Bioinks; cell-laden scaffolds; drug delivery carriers	51-54

(*cont'd...*)

Table 1. (*Continued*)

Material category	Representative materials	Degradability	Bone-regenerative activity	Key advantages	Main limitations	Application scope	References
Synthetic polymers	PCL; PLA; PLGA	Degradable (tunable from months to years)	Weak (surface functionalization required)	Tunable mechanical properties and degradation rate; mature hot-melt extrusion process of PCL, used for macroscopic frameworks of large-segment bone defects; PLA/PCL blending synergistically improves brittleness and cell adhesion.	Bioinert with poor hydrophilicity; local acidification caused by PLGA degradation products; weak cell adhesion; static materials cannot respond to the dynamic needs of bone healing.	Macroscopic scaffold frameworks; non-load-bearing sites	14,55-57
Natural/ synthetic composite polymers	GelMA/ PCL; Sodium alginate/ chitosan/gelatin	Degradable (designable)	Moderate to strong (synergistic effect)	Balances bioactivity and mechanical properties; the ternary composite scaffold (15% gelatin) increased tensile strength from 386 kPa to 693 kPa while maintaining suitable porosity (383–419 μm); GelMA composite system provides an optimized microenvironment for cell proliferation and differentiation.	Complex degradation matching of multi-components; large parameter optimization space; still static scaffolds, unable to temporally respond to the dynamic process of bone healing.	Multi-scenario bone scaffold design	52,58-60
Smart and responsive materials							
Piezoelectric Materials	PVDF/PVDF–TrFE; BNT/ PCL; TPU/ PVDF	Partially degradable (matrix-dependent)	Strong (piezoelectric effect induces electrical signals to promote osteogenesis)	Reconstruction of bionic electrical microenvironment; multi-mechanism synergistic osteogenesis (activating calcium channels, up-regulating Runx2/ BMP-2, regulating immunity); simultaneous antibacterial activity; can be activated by external ultrasound stimulation to avoid growth factor dependence.	Effect depends on continuous weight bearing, fails during immobilization; clinical response stability and individual differences to be systematically evaluated; high brittleness of ceramic-based piezoelectric materials; insufficient clinical translation evidence.	Adjuvant repair of bone defects; combined with ultrasound activation	61-65

(*cont'd...*)

doi: 10.36922/IJB026280296

Table 1. (*Continued*)

Material category	Representative materials	Degradability	Bone-regenerative activity	Key advantages	Main limitations	Application scope	References
Shape memory polymers	PGDA; PLLA–TMC/CHA; BT/PLA; TPU/PVDF	Degradable (matrix-dependent)	Moderate (depends on material itself, or composite active components)	Minimally invasive implantation; adaptive filling; tunable mechanical modulus; designability for four-dimensional printing; can be compounded with piezoelectric materials for dual functions; excellent cycle stability.	Shape recovery often occurs much faster than the weeks-to-months timescale of bone healing; trigger temperature needs to be finely designed (slightly higher than body temperature); mismatch between degradation rate and shape memory function; insufficient clinical translation evidence.	Irregular cavity defects; minimally invasive surgery scenarios	61,66-69
Chemical signal-responsive materials	pH/ROS responsive hydrogels; Enzyme-responsive scaffolds; glucose/ROS dual-responsive hydrogels	Degradable (triggered by microenvironmental signal response)	Strong (temporally regulated osteogenic signals)	Spatiotemporally controllable responsive degradation (endogenously triggered by pH/ROS/enzyme/glucose); actively matches the temporal sequence of bone healing; precise repair for complex pathological microenvironments (diabetes/osteoporosis); cascade release of multiple factors for synergistic treatment; no exogenous stimulation required.	Complex system with potential interference between response elements; interpatient variability in physiological trigger thresholds; long-term stability and safety to be verified; difficult to precisely match response thresholds with physiological signals.	Infectious/metabolic bone defects	70-74

Abbreviations: BCP: Biphasic calcium phosphate; BMP-2: Bone morphogenetic protein 2; BNT: Bismuth sodium titanate; BT: Barium titanate; CHA: Citric acid-modified hydroxyapatite; EBM: Electron beam melting; ECM: Extracellular matrix; GelMA: Gelatin methacryloyl; HA: Hydroxyapatite; LPBF: Laser powder bed fusion; PCL: Polycaprolactone; PGDA: Poly(glycerol dodecanoate) acrylate; PLA: Poly(lactic acid); PLGA: Poly(lactic-co-glycolic acid); PLLA–TMC: Poly(L-lactic acid-co-trimethylene carbonate); PVDF: Poly(vinylidene fluoride); PVDF–TrFE: Poly(vinylidene fluoride-co-trifluoroethylene); RGD: Arginine–glycine–aspartic acid; ROS: Reactive oxygen species; Runx2: Runt-related transcription factor 2; SLM: Selective laser melting; TPU: Thermoplastic polyurethane; β-TCP: Beta-tricalcium phosphate.

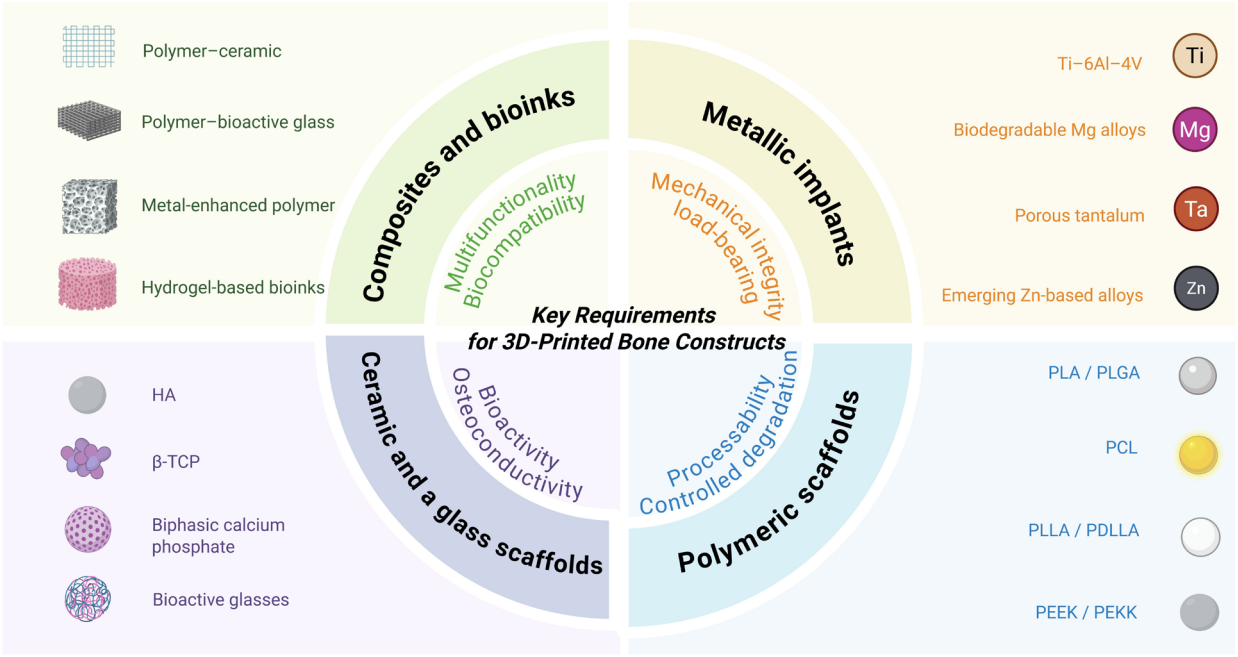


Figure 3. Classification and functional characteristics of materials used for 3D-printed bone constructs. Materials are categorized into composites and bioinks, metallic implants, ceramic and glass scaffolds, and polymeric scaffolds according to their structural and biological functions. Representative materials, including hydroxyapatite, β-tricalcium phosphate, bioactive glasses, titanium alloys, magnesium alloys, tantalum, and biodegradable polymers, provide complementary advantages in mechanical support, bioactivity, processability, and biological regulation. Created in BioRender. Yang, W. (2026). https://BioRender.com/tyty4eo.

Abbreviations: 3D: Three-dimensional; HA: Hydroxyapatite; PCL: Polycaprolactone; PDLLA: Poly(D,L-lactide); PEEK: Polyether ether ketone; PEKK: Polyether ketone ketone; PLA: Poly(lactic acid); PLGA: Poly(lactic-co-glycolic acid); β-TCP: Beta-tricalcium phosphate.

biocompatibility, generally do not react with biological tissues, and primarily provide structural support through their superior mechanical properties. Bioactive ceramics, such as hydroxyapatite (HA) and β-tricalcium phosphate (β-TCP), can chemically interact with biological tissues, promoting bone bonding and regeneration, thereby playing a key role in BTE.

(a) Bioinert ceramics

Bioinert ceramics offer high mechanical strength, wear resistance, and corrosion resistance, making them advantageous for permanent load-bearing implants. Among them, ZrO_2 has attracted particular attention due to its exceptional fracture toughness. Studies have shown that ZrO_2 ceramics fabricated via digital light processing (DLP) can achieve a fracture toughness of 5.25 $MPa{\cdot}m^{1/2}$, significantly higher than other bioceramics.[75] However, bioinert ceramics lack bioactivity and cannot actively promote osteogenesis.[76] Their high chemical stability may induce stress shielding,[29] causing the implant to bear most mechanical load and resulting in disuse-induced bone atrophy in surrounding tissue. Recent efforts have attempted surface functionalization or composite strategies with bioactive ceramics to impart osteogenic activity while retaining mechanical performance,[77] though these approaches remain largely at the experimental stage with limited clinical evidence.

(b) Bioactive ceramics

Bioactive ceramics are the most extensively studied materials in BTE. Their chemical composition closely resembles the inorganic mineral phase of natural bone, and they release bioactive ions during *in vivo* degradation, regulating bone regeneration via specific signaling pathways. Based on composition, bioactive ceramics are classified into calcium phosphate-based and silicate-based ceramics.

- Calcium phosphate-based ceramics:

Hydroxyapatite ($Ca_{10}(PO_4)_6(OH)_2$) closely mimics the crystal structure and chemical composition of natural bone, offering excellent biocompatibility and osteoconductivity.[78] However, its high stability leads to slow degradation, and prolonged occupancy may hinder complete replacement by new bone, affecting biomechanical restoration at defect sites.[79] β-TCP ($Ca_3(PO_4)_2$) degrades faster (months to

years), facilitating bone ingrowth, but its low mechanical strength restricts use to non-load-bearing regions.[80] Biphasic calcium phosphate (HA/β-TCP composite) balances stability and degradability by adjusting the HA/β-TCP ratio, offering potential advantages in bone repair.[81,82]

- Silicate-based ceramics

Silicate bioceramics can release bioactive ions, including Ca^{2+}, Mg^{2+}, and Si^{4+}, that support osteogenic and angiogenic processes. In composite scaffold design, Thangavel and Elsen[83] optimized 3D-printed Mg-Whitlockite (WH)/$CaSiO_3$ (CS) scaffolds using response surface methodology. At WH/CS = 50/50 wt%, 50% infill, and sintering at 1,150 °C, the scaffold achieved 36.74% porosity and 12 MPa compressive strength, balancing mechanical support and osteoinductive potential, with Mg^{2+} enhancing mineralization and Si^{4+} promoting angiogenesis. In preclinical studies, Zhu *et al.*[84] developed injectable, self-setting porous MgO/SiO_2–α-$CaSO_4$ scaffolds (Mg@Ca), which formed *in situ* pores and upregulated *COL1A1* and *BGLAP* via phosphoinositide 3-kinase–protein kinase B (PI3K–AKT) signaling, demonstrating superior trabecular density and bone volume compared to β-TCP in a rabbit femoral head necrosis model.

(c) Bioactive glasses

Bioactive glasses (BGs) are amorphous inorganic materials with tunable compositions and ion-release profiles. Representative systems include 45S5, 58S, and recently developed glass compositions with reduced crystallization tendencies.[85] In physiological environments, BGs undergo surface ion exchange and network dissolution, leading to the formation of an apatite-like interfacial layer that promotes bonding with bone tissue.[86] The release of soluble Si-, Ca-, P-, and other therapeutically active species may further support osteogenic, angiogenic, and immunomodulatory responses. In 3D-printed bone scaffolds, BGs can be used either as the primary scaffold material or as a functional phase incorporated into polymers or metallic implants.[87] Previous studies have shown that 3D-printed BG scaffolds and BG-modified titanium implants can improve osteogenic differentiation and early bone ingrowth.[88] However, brittleness, shrinkage or crystallization during thermal processing, and composition-dependent degradation remain important limitations. Current research therefore focuses on optimizing glass composition and composite design to balance bioactivity, printability, and structural stability.

(d) Mechanisms of bioactive ion regulation

Magnesium ions promote osteogenic differentiation via Notch signaling and protect mesenchymal stem cells from alkaline stress via transient receptor potential melastatin 7/PI3K signaling.[89] Sr^{2+} exerts dual regulation via CaSR, activating Ras/mitogen-activated protein kinase (MAPK) to enhance osteogenesis and inhibiting RANKL/RANK to suppress osteoclast activity.[90,91] Zn^{2+}, an alkaline phosphatase (ALP) cofactor, upregulates Runx2, osteocalcin, and type I collagen via MAPK and PI3K/AKT, and exhibits antibacterial effects at high concentrations.[92] Cu^{2+} activates Wnt signaling to induce vascular endothelial growth factor expression, supporting vascularized bone regeneration.[93] Synergistic effects exist—Mg^{2+}/Sr^{2+} co-administration promotes osteogenesis and angiogenesis;[94] Zn^{2+}/Cu^{2+} combination enhances osteogenic activity while providing an antibacterial microenvironment.[95] Despite their structural biomimicry and ion-mediated bioactivity, the intrinsic brittleness and low fracture toughness of bioactive ceramics limit their load-bearing capacity. Consequently, most bioceramic scaffolds are used for trabecular bone simulation or as bioactive fillers within degradable polymers to balance mechanical support with osteoconductive and osteoinductive functions.

2.2.2. Metallic materials

Metallic materials are widely used for load-bearing bone defect repair due to their high strength and toughness. Additive manufacturing techniques, such as SLM and EBM, enable the fabrication of precisely controlled 3D metal scaffolds,[96] overcoming the mechanical limitations of bioceramics in load-bearing applications. Titanium alloys (e.g., Ti–6Al–4V) exhibit excellent corrosion resistance and fatigue strength, but their high elastic modulus (~110 GPa) exceeds that of cortical bone (15–25 GPa), causing stress shielding and peri-implant bone loss.[29] Biodegradable magnesium alloys have an elastic modulus (40–45 GPa) closer to bone and release Mg^{2+} to promote osteogenesis, but rapid corrosion can generate hydrogen gas and local alkalization before sufficient bone ingrowth.[42] Tantalum is bioinert and non-degradable, but its highly porous interconnected architecture can provide favorable interfaces for bone ingrowth, although its high density and manufacturing costs limit broader clinical use.[48] Surface functionalization (HA coating, anodization, micro-arc oxidation) and alloy optimization (e.g., Mg–Ca, Ti–Nb) partially improve performance.[97,98] These approaches represent incremental improvements rather than fundamental breakthroughs, and metallic biomaterial systems that simultaneously provide controlled degradability, load-bearing capacity, and active osteoinduction have not yet been fully realized.

(a) Titanium alloys

Titanium alloys, particularly Ti–6Al–4V, are widely used for load-bearing bone repair because of their high fatigue

strength and corrosion resistance. Additive manufacturing further enables the fabrication of patient-specific porous lattices with precisely controlled geometries.[99] In addition to architectural design, recent studies have shown that the mechanical performance of titanium can be tailored through process-induced microstructural regulation. For example, Li *et al.*[100] fabricated harmonic-structured pure titanium by laser powder bed fusion, in which spatially heterogeneous grain structures contributed to an improved strength–ductility balance. The study indicates that the performance of additively manufactured titanium can be optimized through the combined control of scaffold architecture and intrinsic material microstructure. Despite these advances, several limitations remain. Dense Ti–6Al–4V has an elastic modulus of approximately 110 GPa, which is substantially higher than that of cortical bone (15–25 GPa).[37] This mechanical mismatch can lead to stress shielding and progressive peri-implant bone loss. Porous lattices fabricated by SLM can reduce the effective modulus to approximately 10–30 GPa, thereby improving mechanical compatibility with cortical bone; however, increasing porosity may compromise fatigue resistance and long-term structural stability.[101] Titanium is also inherently bioinert, and early osseointegration therefore relies largely on mechanical interlocking rather than direct chemical bonding with bone.[102] Surface treatments, such as HA coating, anodization, and micro-arc oxidation, can introduce bioactive interfaces and improve bone–implant interactions.[103] Nevertheless, insufficient coating adhesion and degradation of the coating–substrate interface under prolonged mechanical loading remain important barriers to clinical translation.[104]

(b) Magnesium alloys

Magnesium alloys offer unique advantages in addressing the bioinertia and non-degradability of titanium alloys, with density (1.74–2.0 g/cm^3) and Young's modulus (41–45 GPa) comparable to bone.[105] Importantly, Mg^{2+} can enhance vascularized bone regeneration.[40] However, magnesium alloys can degrade too rapidly relative to the 3–6-month timescale required for complete bone healing, and the associated hydrogen evolution may cause subcutaneous emphysema or impair osseointegration.[106] Rapid degradation can also compromise mechanical integrity before full bone ingrowth, posing early failure risks in load-bearing applications. Alloying strategies have been employed to slow degradation, such as WE43 (Mg-4Y-3RE), in which the addition of rare earth elements yttrium (Y) and neodymium (Nd) followed by heat treatment yields tensile strength of 189.6 MPa and corrosion rate of 0.84 mm/yr,[107] though *in vivo* degradation products (e.g., $Mg_{24}Y_5$, $Mg_{12}YNd$) can activate macrophage NLRP3 inflammasomes, elevating interleukin-1β and interleukin-18 levels and causing fibrous capsule thickening and inflammatory cell infiltration.[108] Recently, interpenetrating phase composite (IPC) strategies have been proposed, in which bioactive secondary phases are infiltrated into additively manufactured porous magnesium scaffolds to integrate mechanical support, degradation control, and biological functionality. Drotárová *et al.*[41] infiltrated calcium phosphate cement into 75% porous WE43 scaffolds to create WE43/HA IPC composites, reducing hydrogen evolution by an order of magnitude and increasing compressive strength from ~15 MPa to 42 MPa (2.8-fold improvement), significantly overcoming material limitations.

(c) Zinc-based alloys

Zinc-based alloys have emerged as promising biodegradable metallic materials for bone implants. Compared with rapidly degrading magnesium-based alloys, zinc-based materials generally exhibit a more moderate degradation behavior, which may provide a better balance between temporary mechanical support and gradual implant resorption.[109] In addition, Zn^{2+} is involved in bone metabolism and may contribute to osteogenic and angiogenic regulation.[44] Laser powder bed fusion (LPBF) enables the fabrication of porous zinc-based implants with customized geometries; however, recent studies have shown that the mechanical and degradation properties of LPBF-fabricated zinc can be affected by build-direction-dependent microstructures.[47] Alloying represents another important strategy for improving the performance of zinc. For example, Zn–Y alloys have demonstrated enhanced osteogenic and angiogenic effects *in vitro* and *in vivo*.[110] Nevertheless, the relatively limited strength of pure zinc, zinc evaporation during laser processing, residual porosity, printing anisotropy, and uncertainties regarding long-term degradation remain important challenges. Future research should therefore focus on the coordinated optimization of alloy composition, printing parameters, and porous architecture.

(d) Tantalum

Tantalum has attracted widespread attention in orthopedic implants due to its excellent corrosion resistance, biocompatibility, and non-toxicity. Its elastic modulus can be adjusted by controlling porosity, and the open internal structure facilitates inward bone growth, thereby accelerating osseointegration.[111,112] Wauthle *et al.*[113] first fabricated high-porosity, fully interconnected pure tantalum implants using SLM, achieving mechanical properties closely matching human bone while supporting bone ingrowth. Studies indicate that scaffolds with ~70% porosity exhibit optimal bone integration, with *in vivo*

experiments showing better bone ingrowth for 70–80% porosity scaffolds compared to 60%, suggesting that approximately 70% porosity may provide a favorable balance for bone integration.[48] In joint revision surgeries, a study of 6,563 total hip arthroplasty patients demonstrated that porous tantalum acetabular components had a 10-year survival rate of 98.9%, superior to fiber-mesh titanium components (97.3%), providing higher initial stability in complex primary and revision cases.[114] Furthermore, combining topology optimization with additive manufacturing enables patient-specific tuning of implant mechanical properties to meet individualized clinical requirements.[111] Nevertheless, widespread clinical adoption of tantalum implants remains limited by its high melting point (2,996 °C), high density (~16.6 g/cm^3),[115] complex processing, and high manufacturing cost. Increasing porosity improves bone integration but inevitably reduces mechanical strength, and the fatigue performance and long-term structural stability of high-porosity scaffolds under cyclic loading still lack sufficient clinical data.

2.2.3. Polymers

Polymers are among the most widely used material classes in 3D printing-based BTE because of their formulation flexibility and broad process compatibility. Natural polymers, such as gelatin, alginate, chitosan, and silk fibroin, effectively support cell adhesion, proliferation, and osteogenic differentiation,[51] but are limited by low mechanical strength and rapid degradation. For example, ionically crosslinked alginate hydrogels are typically brittle with limited mechanical performance[52] and require blending with nanocellulose, synthetic polymers, or chitosan to enhance toughness and stability for load-bearing bone applications. Studies show that combining alginate with cellulose or PCL significantly improves mechanical properties and structural stability, raising the compressive modulus to match trabecular bone (31–48 MPa).[116] High-concentration gelatin methacryloyl (GelMA) provides good print fidelity and structural support, whereas low concentration favors cell viability.[117] Synthetic polymers such as PCL, poly(lactic acid) (PLA), and PLGA allow precise control of degradation rates and mechanical properties, making them primary choices for structural scaffold frameworks. PCL is well-known for toughness, biocompatibility, and non-toxic degradation,[14] and is widely used for macroscopic scaffolds in large bone defect repair. PLA is more brittle, degrades faster, and is less flexible than PCL, but adjusting the PLA/PCL ratio can synergistically mitigate limitations in brittleness, degradation rate, and cell adhesion.[118] PLGA scaffolds face challenges including insufficient mechanical strength, mismatch between degradation and bone healing rates, and limited hydrophilicity and cell compatibility, with printing resolution and precision further constraining applications. Due to inherent conflicts between mechanical performance and bioactivity in single-component polymers, natural/synthetic polymer composites have become mainstream in scaffold design, enhancing biocompatibility, crosslinking capability, mechanical strength, and thermal properties. Singh *et al.*[59] incorporated 15% gelatin into sodium alginate and reported that the resulting 3D-printed ternary composite scaffolds exhibited an increase in tensile strength from 386 ± 15 kPa to 693 ± 15 kPa while maintaining pore sizes of 383–419 μm, controllable degradation, and excellent cell compatibility. Gelatin enhanced cell adhesion via RGD sequences and improved structural stability through electrostatic interactions with the polyelectrolyte network. Although natural/synthetic polymer composites partially address the mechanical-bioactivity trade-off, they remain "static" scaffolds, incapable of dynamically adapting their mechanical support, degradation, or biofactor release to physiological demands during bone healing. This limitation has motivated the development of smart responsive materials. By incorporating stimuli-responsive mechanisms (e.g., pH-triggered drug release, enzyme-mediated degradation, thermally induced shape memory), scaffolds can transition from "passive support" to "active adaptation," releasing bioactive factors, modulating mechanics, or activating osteogenic signals as needed during different stages of bone regeneration, providing improved temporal coordination with the bone-healing process.

2.2.4. Smart and responsive materials

Conventional scaffold materials, including bioceramics, metals, and polymers, share a common limitation: once implanted, their mechanical properties, degradation behavior, and biological signaling become essentially fixed, preventing adaptation to the dynamic physiological environment of bone healing. Bone defect repair, however, is a dynamic process that unfolds over several weeks to months. Smart and responsive materials are characterized by their ability to autonomously or controllably adjust their properties in response to physiological signals at different stages of bone healing, providing dynamic mechanical support and biological functionality aligned with the evolving tissue environment.

(a) Piezoelectric materials

Piezoelectric materials can convert mechanical deformation from daily physiological activity into local electrical signals, mimicking the electromechanical coupling of natural bone to continuously stimulate osteogenesis. Chen *et al.*[119]

recently fabricated a 3D-printed composite piezoelectric scaffold of polyvinylidene fluoride-trifluoroethylene and calcium silicate phosphate, which, after seven days of hydration, exhibited compressive strength of 7.6–8.38 MPa (matching trabecular bone) and a piezoelectric coefficient (d_{33}) of 6.01 pC/N, significantly higher than natural bone (0.7 pC/N), achieving integrated mechanical support, electrical stimulation, and osteoinductive functionality. Ceramic-based piezoelectric materials offer stronger electrical output; for example, a 3D-printed PCL scaffold filled with lead-free bismuth sodium titanate ceramics demonstrated an 88.6% increase in mechanical strength and a 46.3% increase in cell proliferation.[120] However, the inherent brittleness of ceramics has led researchers to adopt polymer-based composites. Li *et al.*[61] developed a thermoplastic polyurethane/poly(vinylidene fluoride-co-trifluoroethylene) dual-function scaffold integrating shape-memory-assisted minimally invasive implantation with *in situ* piezoelectric stimulation, achieving a d_{33} value of 2.47 pC/N, close to the piezoelectric constant of natural bone (d_{33} = 0.7–2.3 pC/N). Notably, the piezoelectric effect of these scaffolds relies on sustained mechanical loading; Dixon *et al.*[121] introduced low-frequency ultrasound as an external trigger to effectively activate scaffold mineralization. Furthermore, the biological effects of piezoelectric materials extend beyond direct osteogenic stimulation. Wang *et al.*[122] combined a 3D-printed potassium sodium niobate/nano-hydroxyapatite/polylactic acid (KNN/nHA/PLA) piezoelectric scaffold with an icariin-loaded GelMA hydrogel; ultrasound-activated piezoelectric stimulation promoted bone formation while icariin induced macrophage M2 polarization, optimizing the immune microenvironment and demonstrating a synergistic strategy integrating ultrasound-triggered piezoelectric activation with targeted immunomodulation. Overall, research on piezoelectric scaffolds is shifting from single-parameter optimization of material piezoelectricity toward systematic integration of multi-signal cues, yet their stability under physiological mechanical loading and interpatient variability and reproducibility under clinical conditions remain critical issues requiring systematic evaluation.

(b) Shape-memory materials

Unlike piezoelectric materials, which rely on mechano-electrical signal transduction, the response of shape-memory materials primarily depends on their ability to recover a programmed shape. These materials typically recover preprogrammed shapes under physiological temperature or specific hydrated environments, enabling early-stage adaptation to irregular defect geometries while providing progressive mechanical support throughout the healing process. For example, Zhang *et al.*[66] developed a poly(glycerol dodecanedioate acrylate) shape-memory polymer with a glass transition temperature precisely tuned within the range of 20 °C–37 °C; upon implantation, body temperature triggered rapid recovery (37 °C, 98% recovery in 0.4 s) with cycle stability exceeding 100 repetitions. Using DLP 3D printing, Yang *et al.*[123] fabricated poly(L-lactic acid)-trimethylene carbonate (PLLA–TMC)/citric acid-modified hydroxyapatite shape-memory scaffolds based on PLLA–TMC and citrate-modified HA, with a glass transition temperature tuned to 37 °C. The scaffolds autonomously recovered their pre-set geometry within 60 s post-implantation, precisely adapting to irregular defect surfaces, and were further functionalized with a tannic acid–magnesium polyphenol coating to achieve antibacterial, immunomodulatory, and osteoinductive effects in an infectious bone defect model. Notably, Lv *et al.*[124] embedded barium titanate piezoelectric nanoparticles into a thermoresponsive PLA-based shape-memory matrix, producing a barium titanate/PLA four-dimensional (4D)-printed scaffold with both shape-memory and piezoelectric functionality. Low-intensity pulsed ultrasound significantly upregulated bone marrow mesenchymal stem cell osteogenic markers, achieving simultaneous shape-adaptive filling and electrically stimulated osteogenesis. However, shape recovery in these materials typically occurs within seconds to minutes post-implantation, whereas mechanical support adjustments required for bone healing span several weeks. Extending the response time window of shape-memory materials to synchronize mechanical evolution with callus maturation remains a critical scientific challenge in this field.

(c) Chemically responsive materials

Chemically responsive materials represent a biologically responsive class of smart scaffolds that can be activated by specific biochemical cues during bone healing. During early-stage bone defect healing, local tissue pH may drop from the physiological value of 7.4 to 6.5–7.0, and reactive oxygen species (ROS) levels rise significantly; as inflammation subsides, the microenvironment gradually returns to near-neutral, and osteogenic signals dominate. These stage-specific biochemical cues provide a natural endogenous "switch" for temporally controlled delivery of therapeutic factors. In pH-responsive strategies, Liu *et al.*[70] utilized local acidic microenvironments to trigger the cascade release of calcium ions, dexamethasone, and zoledronate, achieving integrated microenvironment modulation, osteoinduction, and osteoclast inhibition. Compared to pH signals, enzyme-responsive materials exhibit higher biological specificity; for example, phosphoester bonds sensitive to ALP were introduced

into a poly(propylene fumarate/PCL click-crosslinked network, enabling scaffold degradation rates to actively accelerate in response to ALP upregulation during osteogenic differentiation, fundamentally resolving the temporal mismatch between polymer scaffold degradation and bone formation.[71] To address oxidative stress during inflammation, Chen *et al.*[125] developed $ZnFe_2O_4$ magnetic scaffolds that combine ROS scavenging with static magnetic field-induced osteogenesis, simultaneously quenching free radicals, upregulating RUNX2 and BMP-2 expression, and providing antibacterial activity, thereby bridging the transition from inflammation resolution to osteogenesis. In metabolic bone disease models, Fu *et al.*[72] designed a glucose/ROS dual-responsive enzymatic hydrogel (AAT-ZCG), integrating blood glucose as a novel trigger; the cerium-based nanozyme–glucose oxidase cascade system synchronously cleared ROS, modulated macrophage polarization, and selectively inhibited osteoclasts, offering a new paradigm for precise repair of diabetic bone defects. However, increasing the number of responsive dimensions often exponentially raises system complexity, and issues such as cross-interference between response elements, differences between *in vivo* and *in vitro* kinetics, and variability in response thresholds due to individual metabolic differences remain key challenges in the field.

2.3. 3D printing technologies

Three-dimensional printing technologies used in BTE include extrusion-based printing, inkjet bioprinting, laser-assisted powder bed fusion, photopolymerization, and high-resolution laser-based fabrication (Table 2). These approaches differ substantially in material compatibility, achievable feature size, compatibility with living cells, mechanical performance, and fabrication throughput. No single technique can me*et al*l requirements of bone reconstruction; therefore, the choice of printing method should be matched to the intended structural scale and biological function, while hybrid manufacturing is increasingly used when load-bearing support, cellular organization, and fine interfacial features must be combined within the same construct.

2.3.1. Extrusion-based techniques

Extrusion-based techniques are among the earliest additive manufacturing methods applied in BTE, with representative approaches including FDM and extrusion bioprinting.[126] These methods operate by applying pneumatic or mechanical force to continuously extrude thermoplastic polymers, hydrogels, or composite materials from a printing nozzle, layer by layer, according to a predefined path. The main advantages of extrusion-based printing include broad material compatibility, enabling the use of high-temperature thermoplastics (e.g., PCL, PLA) as well as cell-laden hydrogels at room temperature (e.g., gelatin, alginate), along with low equipment cost, operational simplicity, and the feasibility of multi-material composite printing.[127] However, the resolution is limited by nozzle diameter (typically 100–500 μm), making the direct fabrication of sub-100-μm features challenging. In cell-laden printing, shear forces during extrusion may affect cell viability,[128] requiring a balance between ink rheology and cell survival. Clinically, extrusion-based techniques have demonstrated relatively high translational potential and have been explored in several bone repair applications. A useful extension of conventional extrusion bioprinting is embedded, or suspension-assisted, printing, in which soft or low-viscosity bioinks are deposited within a temporary support medium that stabilizes the printed filaments.[129] This strategy enables the fabrication of free-form hydrogel constructs that would otherwise deform or collapse when printed in air. Freeform reversible embedding of suspended hydrogels is a representative approach, although printing fidelity and construct recovery depend on the rheological compatibility between the bioink and support bath and on effective removal of the supporting material.[130]

2.3.2. Inkjet bioprinting

Inkjet bioprinting is a non-contact, drop-on-demand technique that deposits discrete volumes of bioink through thermal, piezoelectric, or other actuation mechanisms. Unlike extrusion bioprinting, which continuously forms filaments, inkjet printing allows the rapid and spatially controlled placement of cells, biomolecules, and hydrogel precursors while generally imposing only brief mechanical and thermal stresses on the deposited cells.[131,132] Its applicability, however, is constrained by a relatively narrow printable-material window: bioinks must permit stable droplet formation, whereas excessive viscosity or high cell and particle concentrations can lead to irregular droplet generation and printhead clogging.[133] In BTE, inkjet printing has been used to distribute human mesenchymal stem cells and bioactive nanoparticles within photo-crosslinked hydrogel scaffolds, supporting osteogenic differentiation and mineralized tissue formation.[134] Thus, inkjet bioprinting is particularly suited to the precise patterning of cells and bioactive components within or onto an existing supporting matrix, rather than the independent fabrication of large load-bearing bone scaffolds.

2.3.3. Laser-assisted powder bed fusion techniques

Laser-assisted powder bed fusion techniques, including SLS and SLM, operate by selectively scanning powder layers with a high-energy laser, causing localized melting or sintering of particles to form solid structures.[135] This

approach is applicable to metals (e.g., titanium alloys, cobalt–chromium alloys), as well as certain ceramics and polymer powders.[136] The key advantages of laser-assisted powder bed fusion lie in its high resolution (tens of microns) and excellent mechanical properties,[137] enabling the fabrication of complex porous structures with strong load-bearing capacity, particularly suitable for mechanical reconstruction of large bone defects. However, the high-temperature processing precludes direct incorporation of viable cells or bioactive factors, typically restricting this technique to acellular scaffolds. Additionally, high equipment cost, process complexity, and concerns regarding residual metal powder biocompatibility limit its broader clinical adoption.[138]

2.3.4. Photopolymerization-based techniques

Photopolymerization-based techniques primarily include SLA and DLP. These methods operate by selectively curing photosensitive resins with ultraviolet or visible light, building structures layer by layer with high precision. With the development of biocompatible photosensitive resins, photopolymerization has become increasingly applied in BTE.[139] The key advantages of this approach are its ultra-high resolution, reaching a few to tens of microns, enabling the fabrication of complex micro-porous architectures, biomimetic osteons, and even vascular network channels.[140,141] In addition, DLP offers relatively fast printing speeds, suitable for high-throughput scaffold production. Nevertheless, photopolymerization in BTE still faces several challenges: first, material selection is limited to photo-crosslinkable polymer systems (e.g., GelMA, polyethylene glycol diacrylate), with poor compatibility for natural polymers and ceramics; second, the potential cytotoxicity of photoinitiators and unpolymerized monomers restricts cell-laden printing; and third, in conventional SLA and DLP systems, light scattering, optical voxel dimensions, and material-dependent curing behavior generally limit reliable fabrication to the micrometer scale; direct submicrometer or nanoscale structural control requires specialized nonlinear photopolymerization techniques such as two-photon polymerization (TPP).

2.3.5. Two-photon polymerization

Two-photon polymerization, typically performed by femtosecond-laser direct writing, confines photopolymerization to a small focal volume through nonlinear two-photon absorption. This localized reaction enables the fabrication of complex 3D structures with submicrometer features and therefore provides finer structural control than conventional SLA or DLP.[142] In BTE, this capability is particularly useful for constructing defined pore-wall geometries, ECM-like interfaces, and surface topographies that influence cell–material interactions. Fu and Yu,[143] for example, fabricated GelMA-based hydrogel structures with feature sizes below 120 nm and reported favorable cytocompatibility with MC3T3-E1 cells. However, the serial point-scanning process that gives TPP its high resolution also limits build volume and fabrication speed. In addition, suitable photoresists must combine two-photon sensitivity with processability, cytocompatibility, and sufficient mechanical stability, which restricts the available material systems.[144,145] Binder *et al.*[146] addressed the throughput limitation using a resonant-scanner-based system and achieved at least an order-of-magnitude increase in the fabrication rate of tissue-engineering micro-scaffolds. TPP is therefore currently better suited to localized high-resolution features, research-scale micro-scaffolds, and high-resolution components within hybrid multiscale constructs than to the stand-alone fabrication of clinically sized load-bearing bone implants.

In practice, a single technique (extrusion-based, laser-assisted powder bed fusion, or photopolymerization-based) is often insufficient to meet the requirements for multiscale construction spanning macro, micro, and nanoscale levels. Consequently, multi-technology integration strategies are emerging as a key direction in 3D printing-based BTE. For instance, extrusion-based printing can be combined with photopolymerization to fabricate the macroscopic scaffold body and the micro-biomimetic interface, respectively; alternatively, laser-assisted powder bed fusion can be used to produce a high-strength metal framework, which is then coupled with extrusion-based bioprinting of cell-laden hydrogels, achieving synergistic optimization of mechanical performance and biological functionality (Figure 4).

3. 3D reconstruction of bone tissue

3.1. Cross-scale coupling and design logic

Native bone is organized as a hierarchical system in which anatomical geometry, tissue architecture, ECM organization, and molecular signaling are functionally interconnected

Table 2. Comparison of mainstream 3D printing technologies for bone tissue engineering

Technology category	Technology and working principle	Fabrication range and resolution	Typical applied materials	Reference mechanical properties	Cell compatibility	Key advantages	Main limitations	Clinical translation potential	References
Extrusion-based forming									
Fused deposition modeling	Thermoplastic filaments are melted and extruded, followed by layer-by-layer deposition.	100–700 μm; centimeter to decimeter scale	PCL, PLA, PLGA, PEEK, and composites (e.g., PCL/HA, PCL/PLA)	Pure PCL scaffolds: 4–77 MPa (dependent on porosity); further enhanced by composite reinforcement	Not applicable to direct cell printing; cells can be seeded after printing, depending on material and surface properties.	Low equipment cost; wide material compatibility; multi-material/ gradient printing; mature process; numerous FDA-approved products	Low printing accuracy; weak interlayer bonding; thermal degradation of thermosensitive materials; prone to nozzle clogging	Widely applied in orthopedic implants	126,147-151
Extrusion-based bioprinting	Hydrogels or bioinks are extruded via pneumatic/ mechanical force.	> 100 μm (limited by nozzle diameter); centimeter-scale construction	Gelatin, alginate, GelMA, collagen, cell-laden bioinks	Pure hydrogels: compressive modulus 1–100 kPa (typical 7.8 kPa); with composite reinforcement Young's modulus up to 50–200 MPa	40–90% (varies with shear stress; > 90% under optimized conditions); relatively established use in medical-device and scaffold manufacturing	Live cell loading capability; broad material compatibility; gradient structure fabrication; mild printing conditions	Low printing accuracy; impaired cell viability from shear stress; strict rheological requirements; post-crosslinking required	Extensive preclinical studies; a few candidates in clinical trials	152-155
Laser-assisted powder bed fusion									
Selective laser melting	Metal powders are fully melted by laser and solidified layer by layer.	30–200 μm; centimeter to decimeter scale (load-bearing metal implants)	Ti–6Al–4V, Ta, Co–Cr, Mg alloys	Tensile strength: 900–1200 MPa; Elastic modulus: 110 GPa	Not applicable to direct cell printing; post-printing cell responses depend on alloy composition and surface treatment.	Dense forming structure; excellent mechanical properties; complex porous TPMS structure fabrication; clinically mature	High equipment cost; high residual stress; heat treatment required; strict requirement for powder sphericity	High (widely applied in load-bearing orthopedic implants)	156-159

(*cont'd...*)

Table 2. (*Continued*)

Technology category	Technology and working principle	Fabrication range and resolution	Typical applied materials	Reference mechanical properties	Cell compatibility	Key advantages	Main limitations	Clinical translation potential	References
Selective laser sintering	Polymer/ceramic powders are selectively sintered (not fully melted) by laser; unmelted powder acts as natural support structure.	10–120 μm; centimeter-scale porous scaffolds	PCL, PA, TPU, HA, ceramic/polymer composite powders	Compressive strength: 0.6–38.7 MPa (tunable via porosity and structural design)	Not applicable to direct cell printing; post-printing cytocompatibility is material- and surface-dependent.	Support-free fabrication; high material utilization; suitable for large-scale porous structures	Rough surface; low relative density; weak interlayer bonding; inferior mechanical properties compared to selective laser melting	Translation is material- and device-specific; degradable selective laser sintering-fabricated scaffolds for bone tissue engineering remain predominantly at the preclinical stage.	160-163
Photopolymerization									
Stereolithography	A laser scans liquid photocurable resin layer by layer to induce site-specific photopolymerization and solidification.	25–100 μm; micrometer-to-centimeter scale (dental or customized structures)	Photocurable resins, ZrO_2/HA ceramic slurries, PEGDA, GelMA	Photocurable resins: tensile strength 3.3–51 MPa, compressive strength 15.6–29.1 MPa; ZrO_2 ceramics: flexural strength 755–1150 MPa	Native resins mostly cytotoxic; > 90% viability after optimized post-processing	High printing accuracy and excellent surface quality; bioceramic scaffold fabrication; CT-based customized fabrication	Restricted to photocurable material systems; support structure required; debinding and sintering needed for ceramic printing	Mature dental applications; preclinical stage for orthopedic applications	164-168
Digital light processing	Ultraviolet light patterns are projected via a digital micromirror device to cure an entire layer of photocurable resin in a single exposure, achieving layer-by-layer fabrication.	15–100 μm; micrometer-to-centimeter scale (high-throughput or TPMS structures)	ZrO_2, HA, β-TCP ceramic slurries; PEGDA, GelMA; shape memory materials	Tensile strength: 20–60 MPa; mechanical properties tunable via additives and fiber reinforcement	> 90% (with biocompatible photoinitiator and optimized post-processing)	Fast printing speed; capable of processing high-solid-content ceramic slurries; suitable for 4D printing; TPMS structure fabrication	Restricted to photocurable material systems; support structure required; peeling forces can hinder large-scale fabrication	Mature dental applications; at the large-animal study stage for orthopedic applications	140,169-172

Abbreviations: 3D: Three-dimensional; 4D: Four-dimensional; CT: Computed tomography; FDA: Food and Drug Administration; GelMA: Gelatin methacryloyl; HA: Hydroxyapatite; PA: Polyamide; PCL: Polycaprolactone; PEEK: Polyether ether ketone; PEGDA: Polyethylene glycol diacrylate; PLA: Poly(lactic acid); PLGA: Poly(lactic-co-glycolic acid); SLS: Selective laser sintering; TPMS: Triply periodic minimal surface; TPU: Thermoplastic polyurethane; β-TCP: Beta-tricalcium phosphate.

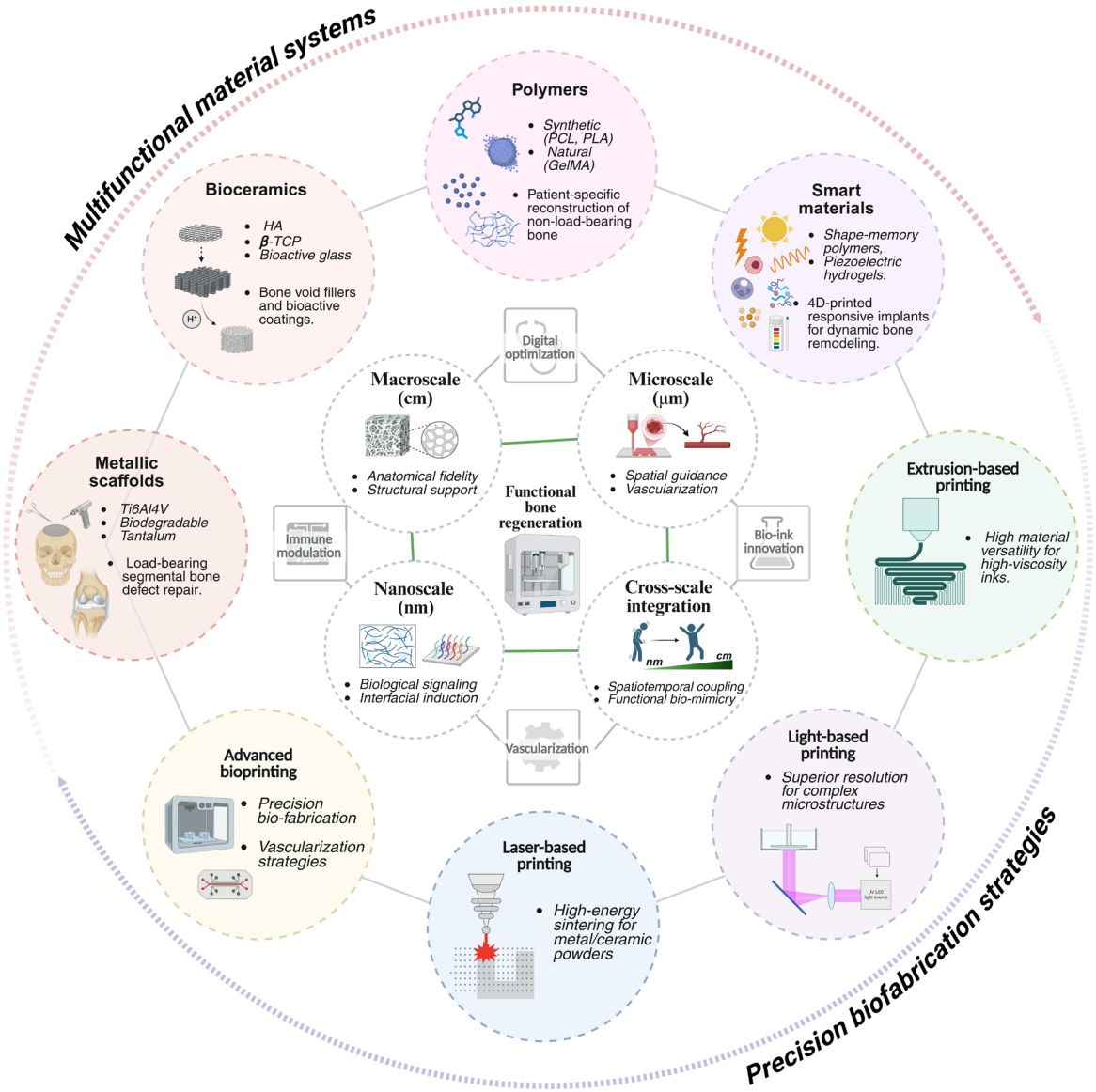


Figure 4. A comprehensive framework of multiscale 3D printing strategies for bone tissue engineering. The framework illustrates the integration of functional materials, fabrication technologies, and hierarchical structural regulation across multiple length scales. Macroscale reconstruction provides anatomical matching and mechanical support, microscale engineering regulates cellular organization and vascularization, and nanoscale engineering modulates biological signaling and cell–material interactions. Different printing approaches, including extrusion-based printing, light-assisted printing, laser-based printing, and advanced bioprinting techniques, contribute to cross-scale integration for functional bone regeneration. Created in BioRender. Yang, W. (2026). https://BioRender.com/tyty4eo.

Abbreviations: 4D: Four-dimensional; β-TCP: Beta-tricalcium phosphate; GelMA: Gelatin methacryloyl; HA: Hydroxyapatite; PCL: Polycaprolactone; PLA: Poly(lactic acid).

across multiple length scales.[173] Accordingly, multiscale reconstruction should not be understood as the simple coexistence of macroscopic, microscopic, and nanoscale features within a single scaffold. Rather, design variables at one scale constrain, and are functionally coupled to, those at other scales. Macroscale geometry and bulk mechanics define the boundary conditions for implantation and load transfer; microscale pores, fibers, and channels regulate local stress distribution, cell organization, vascular ingrowth, and mass transport; and nanoscale surface and biochemical cues influence protein adsorption, cell adhesion, immune responses, and osteogenic signaling.

Effective bone regeneration therefore requires coordinated optimization across scales rather than independent optimization of individual structural parameters.[174] In this context, the primary challenge of 3D printing-based bone regeneration is not merely achieving higher spatial resolution, but establishing functional coupling between structural hierarchy, mechanical behavior, mass transport, and biological regulation across scales.

These cross-scale interactions generate inherent design trade-offs. At the macro- and microscales, increasing porosity or pore interconnectivity can enhance cell infiltration, nutrient diffusion, and vascular ingrowth, but may simultaneously compromise compressive strength, fatigue resistance, and structural stability. Conversely, increasing strut thickness or material density can improve load-bearing capacity while restricting mass transport and tissue penetration. Pore size and porosity should therefore be regarded as context-dependent design variables rather than universal criteria, with their preferred ranges determined by material properties, anatomical location, loading conditions, fabrication method, and biological requirements. Gradient architectures, topology optimization, and biomimetic lattice designs offer practical strategies for reconciling these competing demands by spatially integrating mechanically robust regions with highly porous regenerative domains.[173,175] Microscale organization further defines the local environment in which nanoscale biological regulation occurs. Pore walls, printed fibers, and perfusable channels determine surface area, curvature, fluid shear, and cellular distribution, thereby affecting protein adsorption and cellular responses to nanoscale topography, mineral phases, adhesive ligands, and released ions. Conversely, nanoscale functionalization can influence higher-scale performance. For example, nano-HA, BG nanoparticles, and other nanophases may enhance mineralization and osteogenic signaling, but can also alter ink rheology, particle dispersion, interfacial bonding, degradation behavior, and printing fidelity.[176-178] Thus, modifications at any individual scale should be evaluated in terms of their system-level consequences for mechanics, transport, processability, and biological function.

Cross-scale integration can be achieved through three complementary design routes. The first is hierarchical structural design within a single manufacturing process, using controlled toolpaths, lattice geometry, spatial gradients, or biomimetic architectures to coordinate macro- and microstructure. The second is hybrid fabrication, in which technologies with different material and resolution capabilities are combined; for example, a load-bearing metallic or thermoplastic framework produced by powder-bed fusion or FDM may be integrated with cell-laden hydrogels through extrusion bioprinting. Sacrificial, embedded, coaxial, or multicellular printing can further introduce perfusable channels and spatially organized cellular compartments. The third is functional integration, in which cells, growth factors, bioactive ions, nanoparticles, or immunomodulatory components are selectively incorporated into the construct, including through post-printing mineralization, coating, or surface modification. Such approaches enable nanoscale interfacial functionality to be introduced without requiring the entire scaffold to be fabricated at nanometer resolution. Representative studies have incorporated Haversian-like channels, multicellular delivery systems, Voronoi-type architectures, hollow-fiber networks, and nano-apatite coatings to reproduce distinct aspects of hierarchical bone organization.[175,178,179] These strategies are not mutually exclusive, and their selection should be dictated by the anatomical, mechanical, vascular, and biological requirements of the target defect rather than by printing resolution alone.

Despite these advances, most current studies integrate only two length scales or examine individual design parameters in isolation. Quantitative relationships linking macroscale mechanics, microscale transport and cellular organization, and nanoscale signaling remain poorly defined. Moreover, improvements at one scale may introduce adverse effects at another, as illustrated by the loss of mechanical stability associated with excessive porosity or the deterioration in printability caused by nanoparticle incorporation. Future multiscale scaffold design therefore requires experimentally validated cross-scale models and multi-objective optimization frameworks that simultaneously consider anatomical matching, mechanical performance, mass transport, degradation, vascularization, and biological signaling. The following sections examine design principles and representative strategies at the macro-, micro-, and nanoscale levels before considering their integration in hierarchical bone reconstruction.

3.2. Macroscale 3D reconstruction of bone tissue

At the macroscale, native bone functions as a natural functionally graded composite, in which coordinated integration of cortical and cancellous bone enables optimal mechanical performance and physiological function (Figure 5A). This hierarchical organization allows bone to simultaneously meet load-bearing and metabolic demands, representing an efficient biological design. Cortical bone forms the dense outer shell and diaphysis of long bones, accounting for approximately 80% of total bone mass. It consists of tightly packed osteons arranged in concentric lamellae, creating a compact tubular or

plate-like architecture that provides high mechanical strength and resistance to deformation. However, its low porosity limits mass transport and nutrient exchange, resulting in relatively low metabolic activity. In contrast, cancellous bone is primarily located in the epiphyses of long bones, vertebral bodies, and flat bone interiors. Its interconnected trabecular network forms a highly porous 3D structure that facilitates efficient load distribution, impact absorption, and weight reduction. Importantly, cortical and cancellous bone are seamlessly integrated through continuous gradients in structure, composition, and mechanical properties rather than existing as isolated compartments. This macroscale architecture maximizes mechanical efficiency and physiological functionality while minimizing material usage, providing a key biological blueprint for macroscale bone reconstruction in 3D printing-based BTE.

At the macroscale, integrated structure–function design has become a central paradigm in the development of 3D-printed bone scaffolds, markedly improving fabrication feasibility and potential for clinical translation.[180] By integrating patient-specific imaging data with digital modeling and layer-by-layer fabrication, 3D printing enables individualized and functional reconstruction of large, complex bone defects at the macroscale. Compared with conventional grafts, this approach allows direct mapping of personalized geometry and tunable mechanical parameters onto the implant.[14] In recent years, numerous studies have systematically demonstrated the feasibility and advantages of 3D printing for macroscale bone construction. Zhang *et al.*[181] employed a low-cost and process-stable FDM technique to fabricate PLLA/nano-HA composite scaffolds with patient-specific external geometry and high nano-HA content. The scaffolds precisely matched defect contours and exhibited macroscopic mechanical properties suitable for surgical implantation, with compressive strength exceeding that of native cancellous bone. In a complementary animal approach, Lee *et al.*[88] utilized SLM to produce Ti–6Al–4V implants incorporated with 58S BG. Both BG coating and

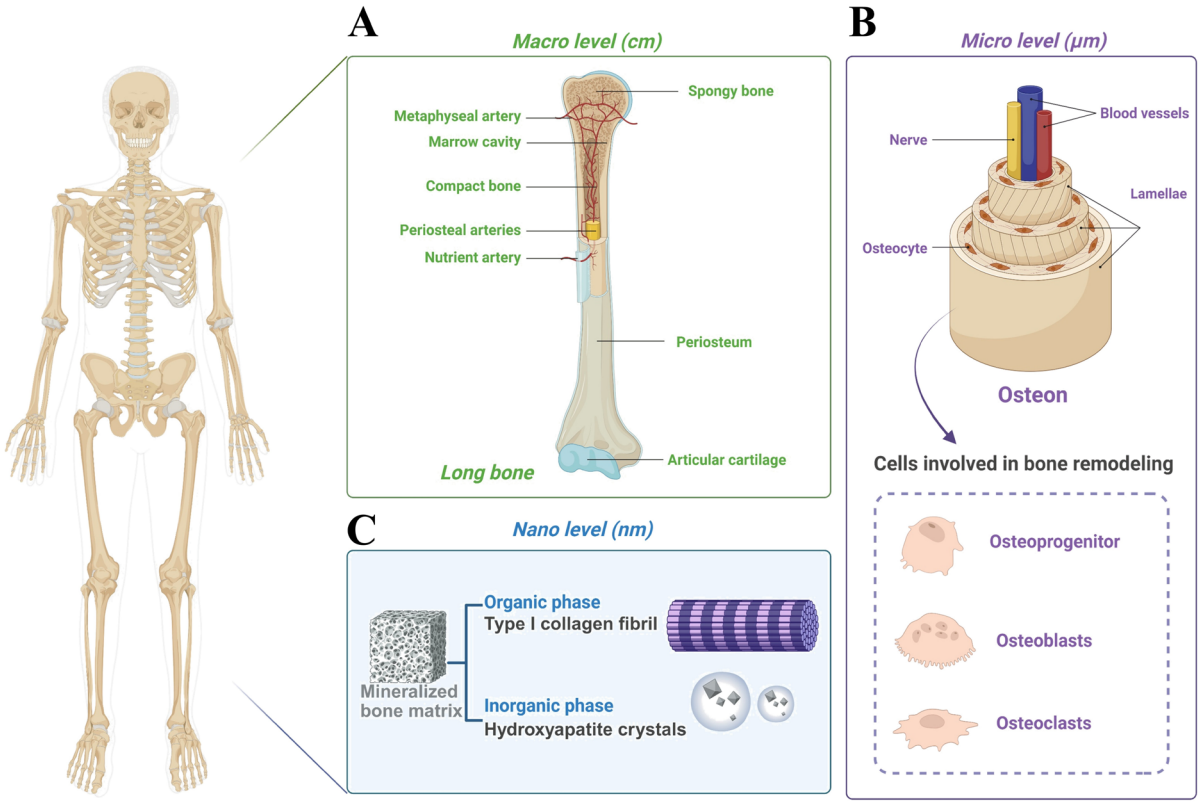


Figure 5. Hierarchical organization of native bone tissue across macro-, micro-, and nanoscale levels. (A) Macroscale architecture of bone, showing the organization of cortical and cancellous regions. (B) Microscale structure of bone, including osteons, vascular channels, and bone-remodeling cells. (C) Nanoscale composition of mineralized bone matrix, characterized by collagen fibrils and hydroxyapatite crystals that provide mechanical reinforcement and biological cues. Created in BioRender. Yang, W. (2026). https://BioRender.com/tyty4eo.

bulk incorporation strategies significantly accelerated early-stage bone ingrowth, as evidenced by increased bone–implant contact and bone density. A representative study combined a macroscopic 3D-printed PLA/HA composite scaffold with electromagnetic field stimulation for repairing rat critical-sized calvarial defects.[182] The scaffold provided suitable mechanical support and a porous architecture, while electromagnetic field treatment enhanced bone marrow mesenchymal stem cell proliferation and osteogenic differentiation via MAPK-related signaling pathways, demonstrating the potential of integrating 3D-printed scaffolds with biophysical stimulation for craniofacial bone regeneration (Figure 6A).

In clinical applications, Ebel *et al.*[183] evaluated the use of in-house 3D printing technology to fabricate personalized polymethyl methacrylate cranial implants. The technology achieved excellent intraoperative fitting accuracy, even for complex frontotemporal orbital defects, and demonstrated significant cost-effectiveness, underscoring potential cost and workflow advantages of 3D printing in clinical treatments. In another clinical case series of 16 patients, patient-specific poly(methyl methacrylate) implants were fabricated intraoperatively using customized 3D-printed molds derived from preoperative CT-based 3D modeling.[184] The approach enabled accurate reconstruction of skull defects with good cranial symmetry, high patient satisfaction, and no postoperative complications, demonstrating that 3D printing-assisted customized molds can be used for cranial defect reconstruction (Figure 6B). Methodologically, modular and resorbable patient-specific scaffold workflows have been developed to integrate surgical constraints with successful feasibility validation in three clinical cases.[185] For complex limb fractures and segmental bone defects, 3D printing-assisted personalized steel plates facilitated shorter surgical times, faster bone healing, and improved joint function recovery. This benefit is attributed to preoperative precision planning and highly conformal intraoperative fixation, providing macroscale clinical benefits. Additionally, Liang *et al.*[186] demonstrated that, in five cases of complex limb fractures, the 3D printing group showed significant improvements in surgical time, bone healing, joint function scores, and postoperative recovery compared to the conventional group. This study confirmed that 3D printing can enable precise preoperative planning and enhance bone healing and functional recovery, further validating the clinical applicability and translational potential of this technology for complex fracture and segmental defect reconstructions.

Although significant progress has been made in the application of 3D printing technology for anatomical bone reconstruction and mechanical support at the macroscale, the internal environment of the macroscopic scaffold remains biologically inert, lacking precise regulation of cellular behavior and metabolic needs. This is particularly problematic in the repair of large bone defects, where the core of the scaffold is prone to issues such as cell death, insufficient nutrient transport, and delayed vascularization. As a result, research focus is gradually shifting from the mechanical biomimicry of macrostructures to the construction of cellular microenvironments at the microscopic scale.

3.3. Microscale 3D reconstruction of bone tissue

Natural bone tissue at the microscale is a complex system consisting of organized functional units, ECM, and active cells (Figure 5B). In cortical bone, osteons are made up of a central Haversian canal surrounded by concentric lamellae, interconnected by Volkmann's canals, forming a 3D network of blood vessels and nerves. This structure enables high compressive and bending strength while maintaining metabolic activity. Trabecular bone consists of trabeculae arranged in plate-like or rod-like structures, forming an efficient porous network that supports load-bearing and facilitates bone marrow and vascular function. The functionality of osteons and trabeculae relies on the ECM, a natural composite made up of organic and inorganic phases. The organic phase consists mainly of type I collagen fibers, which form a flexible framework providing tensile strength. The inorganic phase is primarily composed of HA crystals, which are oriented along the collagen fibers to provide rigidity and compressive strength. Based on the understanding of the microscopic structure, the main objectives of 3D printing in BTE include mimicking bone microarchitecture and ECM-associated organization, creating scaffolds with fibrous or network-like microstructures, and reproducing the spatial organization of natural bone. Therefore, microscale reconstruction aims not only to reproduce geometric features but also to establish functional cellular and vascular microenvironments that support tissue maturation.

With the advancement of multi-material printing, suspended printing, and photocuring technologies, researchers are now able to systematically validate the biological performance and regenerative potential of these constructs both *in vitro* and *in vivo*.[173] Recent studies show that 3D printing can precisely simulate the porous and fibrous ECM structure of natural bone at the microscopic scale, which can enhance osteoblast adhesion, migration, and differentiation.[187,188] Some researchers have co-printed osteoblasts and endothelial cells in scaffolds or introduced hollow perfusable channels to provide a template for vascular regeneration, which significantly

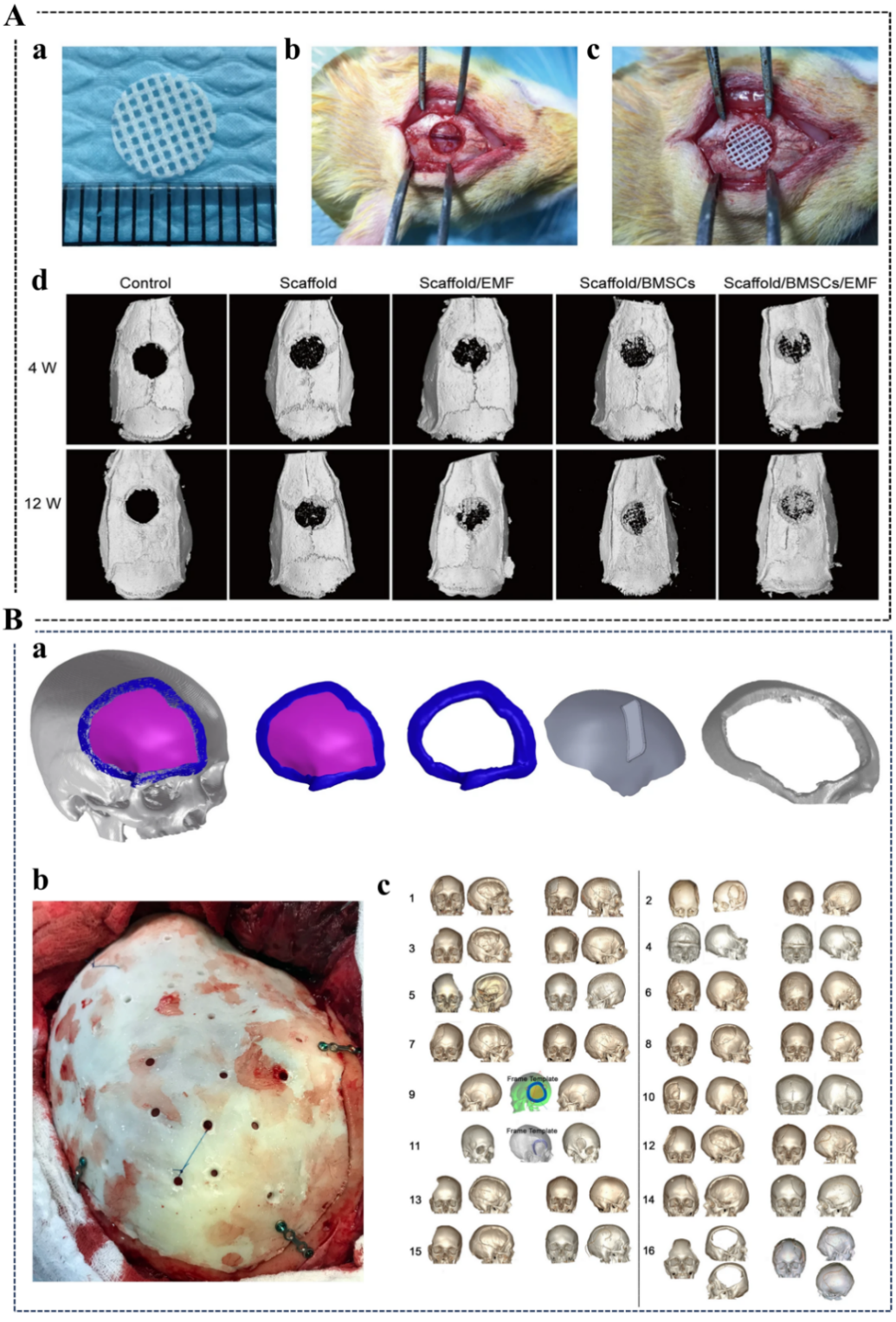


Figure 6. Macroscale 3D reconstruction of bone tissue. (A) Construction of a rat critical-sized calvarial defect and representative reconstructed micro-computed tomography images of crania from different groups at 4 and 12 weeks. Reprinted from Ref.[182] (B) Cranioplasty with a three-dimensional customized mold.[184] a. Reconstructed skull showing craniectomy margins (blue) and implant sketch (pink). b. The implant was fixed over the defect using mini titanium plates. c. Pre-operative and post-operative coronal and sagittal views are shown for each patient. Reprinted from Ref.[184]

improves cell activity and vascularization in the central region.[189] Zhu *et al.*[190] designed and fabricated a structured scaffold for facilitating tendon-to-bone repair (Figure 7A) by offering a structurally and compositionally appropriate microenvironment for healing. In addition, functionalized 3D-printed scaffolds, such as PCL/β-TCP and HA/PLGA composites, can promote osteoblast proliferation and upregulate osteogenic genes, while also supporting the formation of tubular structures by endothelial cells.[191] Zhang *et al.*[179] successfully fabricated a bone-mimicking scaffold with integrated hierarchical Haversian bone structure via DLP-based 3D printing (Figure 7B). Additionally, Laubach *et al.*[175] validated the *in vivo* regenerative potential of a Voronoi-based 3D-printed medical-grade PCL–HA scaffold in a T-cell-deficient CBH-rnu/Arc nude mouse ectopic transplantation model. Histological and scanning electron microscopy results showed that bone cells were distributed along the scaffold pore walls and interconnected through extensions, forming a microstructure continuous with the host bone. A multicenter randomized controlled trial evaluated the safety and efficacy of this specific low-temperature-printed Mg–PLGA–TCP scaffold for the treatment of critical-sized bone defects.[26] The study provided early clinical evidence for the feasibility of this scaffold, although larger patient cohorts and longer follow-up periods are required to evaluate its long-term effectiveness and safety. These achievements demonstrate the translational potential of structurally controllable, compositionally optimized 3D-printed scaffolds and support further clinical evaluation of selected scaffold systems, while laying the groundwork for continued advances in microstructural optimization and functional printing. However, to fully capture the complexity of bone tissue's mechanical properties and biological activity, it is essential to transition from the microscopic to the nanoscale. At the nanometer level, the organization of material units, interfacial interactions, and molecular architecture intricately define the physical and biological properties of bone. The mechanical properties of bone and the cellular responses it elicits are not determined solely by its microscale structure; rather, they are strongly influenced by the precise arrangement and interactions of nanoscale components. This progression from nanostructure to tissue function highlights the deep integration of structure and function in biological materials, which is key to advancing both micro- and nanoscale design in 3D printing for bone regeneration.

3.4. Nanoscale engineering integrated with 3D printing

At the nanoscale, native bone is characterized by a highly organized organic–inorganic composite architecture composed primarily of type I collagen fibrils and HA nanocrystals (Figure 5C). Collagen molecules assemble into fibrils with a characteristic periodic banding pattern, within which plate- or needle-like HA crystals nucleate and align preferentially along the collagen fibril axis rather than being randomly distributed. This hierarchical mineralized collagen structure combines the toughness and crack resistance of the organic matrix with the stiffness and compressive strength of the mineral phase. Interfacial interactions between collagen and HA, including hydrogen bonding, electrostatic interactions, and chemical coordination, further facilitate stress transfer across the organic–inorganic interface and contribute to the distinctive combination of strength, stiffness, and toughness exhibited by bone. Beyond mechanical reinforcement, nanoscale surface roughness, fibrillar orientation, mineral organization, and interfacial chemistry also provide instructive biological cues. Cells sense these nanoscale physical and chemical features through adhesion receptors such as integrins, thereby activating downstream signaling pathways that regulate adhesion, spreading, proliferation, migration, and osteogenic differentiation. The nanoscale organization of bone therefore serves not only as a structural determinant of mechanical performance but also as a biologically active interface that mediates cell–matrix signaling. In the context of 3D printing, nanoscale engineering can be broadly divided into two conceptually distinct strategies. The first is direct high-resolution fabrication, in which the manufacturing process itself physically defines submicrometer or nanoscale structural features. The second is nanoscale material and interfacial functionalization, in which nanostructured components, coatings, or surface features are incorporated into conventionally printed constructs to modulate cell–material interactions. This distinction is important because most extrusion-, inkjet-, and conventional photopolymerization-based systems used in BTE operate predominantly at micrometer-scale resolution or above and therefore do not directly fabricate nanometer-scale architectures throughout the construct.

Among direct high-resolution fabrication techniques, TPP, also termed two-photon lithography or direct laser writing, offers one of the most established routes to 3D submicrometer structural control.[192] In TPP, nonlinear two-photon absorption confines polymerization to a highly localized focal volume, enabling the fabrication of complex 3D structures with submicrometer features and, under optimized conditions, nanoscale feature dimensions.[193] However, the high spatial resolution of TPP is typically accompanied by limited build volume, restricted material compatibility, and relatively low throughput, which constrain its application to clinically

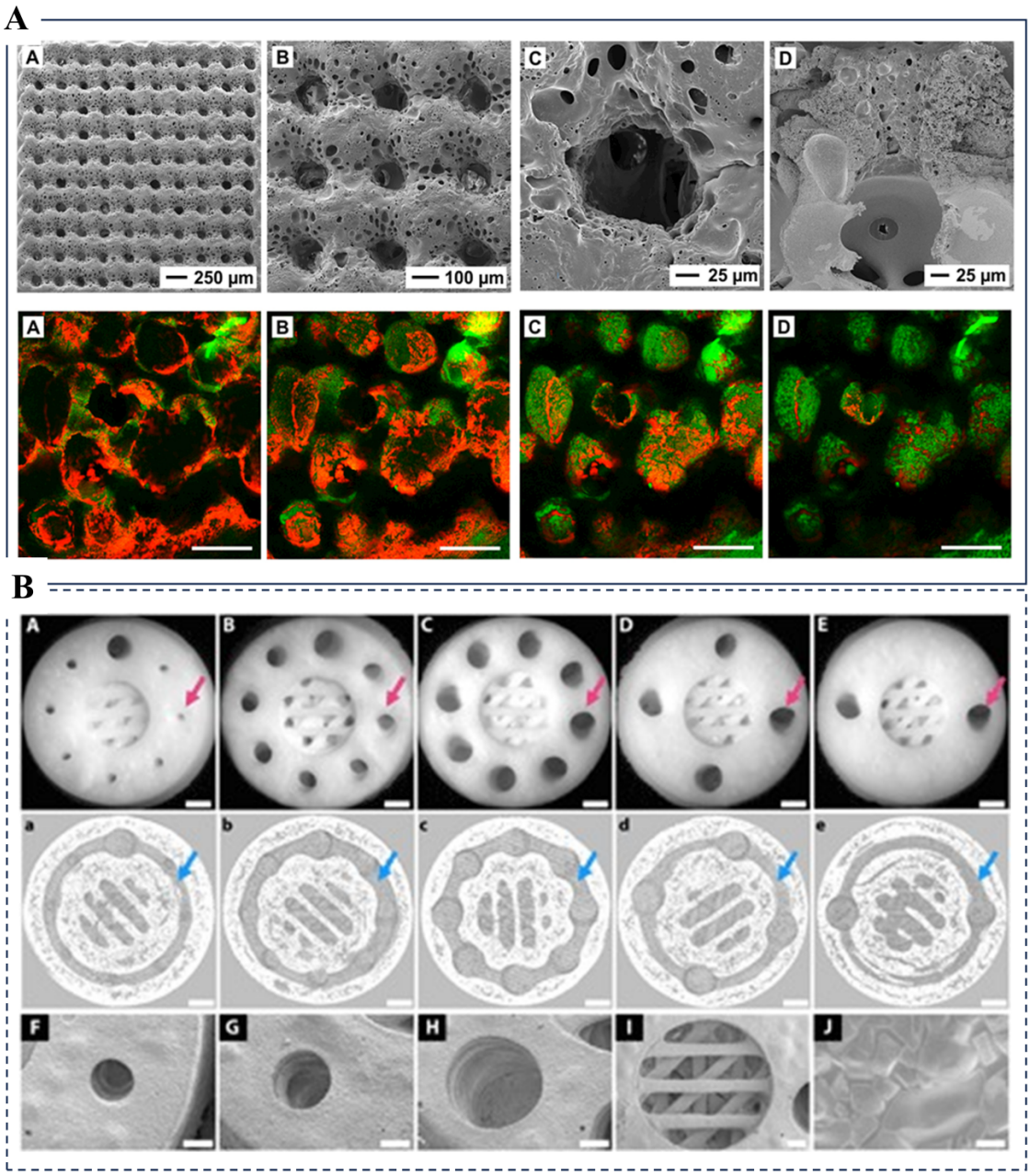


Figure 7. Microscale 3D reconstruction of bone tissue. (A) Transmission electron microscopy images of a layered scaffold structure, with fluorescence images of adipose-derived stromal cells cultured on the scaffold for 28 days. Reprinted with permission from Ref.[190] Copyright © 2018 WILEY-VCH Verlag GmbH & Co. KGaA, Weinheim. (B) 3D printing of bioceramic scaffolds mimicking cortical and cancellous bone structures. Reprinted from Ref.[179]

relevant bone constructs. Recent advances, such as the resonant-scanner-based TPP system developed by Binder *et al.*,[146] have substantially increased fabrication speed and illustrate ongoing efforts to address these limitations. Melt electrowriting (MEW) similarly enables highly controlled deposition of fine polymer fibers and is increasingly used to fabricate ordered cell-scale fibrous networks for tissue engineering.[194] Nevertheless, MEW is generally regarded as a high-resolution microscale fabrication technique rather than a routine nanometer-resolution printing platform.[195] Direct nanoscale fabrication therefore remains largely restricted to specialized technologies and relatively small fabrication volumes.

A more widely applicable strategy is to introduce nanoscale functionality into scaffolds that are themselves fabricated at the macro- or microscale. For example, Yun *et al.*[176] combined extrusion-based 3D printing with low-temperature thermally induced phase separation to produce hierarchical PLA scaffolds containing nanofibrous surface features. In this system, nanoscale morphology arose from phase separation rather than from the spatial resolution of extrusion printing itself (Figure 8A). Likewise, nano-HA, nano-BG, nanosilicates, and other nanostructured components can be incorporated into printing formulations or deposited onto scaffold surfaces to reproduce ECM-like physicochemical cues.[177] Hu *et al.*[196] employed nanofibrous microspheres as hierarchical building blocks for porous scaffold construction (Figure 8B). Nanocomposite bioinks containing nanosilicates or HA have also been investigated for their ability to regulate cell adhesion, osteogenic differentiation, matrix mineralization, and immune responses.[197-200] Surface mineralization, nanoparticle coating, and post-printing nanostructuring can further introduce localized biochemical and topographical signals without requiring the entire scaffold to be fabricated at nanometer-scale resolution. These approaches are therefore more appropriately described as nanoscale material engineering, interfacial functionalization, or nanoscale biological regulation integrated with 3D-printed constructs.

Overall, current 3D printing technologies do not routinely enable the fabrication of clinically sized bone scaffolds with uniform nanometer-scale resolution throughout the entire construct. Conventional extrusion, FDM, inkjet printing, SLA, and DLP primarily operate from the micrometer scale upward, whereas specialized techniques such as TPP can provide localized submicrometer or nanoscale control at the expense of throughput, material versatility, and build size. Consequently, most nanoscale strategies in BTE rely on coupling macro- or microscale additive manufacturing with nanostructured materials, surface engineering, or complementary post-processing. In this review, "direct nanoscale fabrication" therefore refers specifically to processes that physically define nanoscale structural features during fabrication, whereas "nanoscale engineering" is used more broadly to describe nanoscale material, surface, and interfacial regulation integrated with 3D-printed bone constructs.

4. Challenges and future perspectives

Multiscale 3D printing-based BTE aims to integrate patient-specific architecture, hierarchical structural design, and bioactive materials to enable functional, vascularized, and regenerative bone repair (Figure 9). Despite the remarkable progress made in 3D printing technology for BTE, current research shows that achieving clinically functional bone regeneration remains a significant challenge.[173,201] In terms of multi-scale structural integration, while existing technologies have enabled individualized shape matching at the macroscopic level, the engineering of porous structures at the microscopic scale, and the introduction of mineral components at the nanoscale, the coupling between these scales remains insufficient.[174] Most studies continue to focus on optimizing individual scales independently, while systematic strategies for quantitative cross-scale integration remain insufficient.[178,202] This results in printed scaffolds that struggle to simultaneously meet the demands for mechanical support, cellular microenvironment regulation, and bioactivity at nanoscale interfaces. Addressing these cross-scale dependencies therefore remains a central challenge in the design of functionally integrated bone constructs.

At the materials level, although composite ink strategies offer new strategies for multifunctional integration, challenges such as interfacial compatibility among constituent materials, degradation synchronization, and dynamic matching of mechanical and biological properties remain core bottlenecks. For example, ceramic-polymer composite systems often face issues like phase separation, sintering shrinkage, and interface cracking, while natural-synthetic hybrid materials encounter challenges in controlling degradation rates and loss of mechanical performance *in vivo*. These problems not only affect the structural stability of the constructs but also weaken their long-term biological function. Additionally, maintaining the activity of biological components (such as cells, growth factors, and exosomes) during the printing process and achieving precise spatial distribution still present technical difficulties. The concept of "printing and growing" has not yet been fully validated in complex *in vivo* environments.

More critically, 3D printing-based BTE has yet to achieve substantial advances in two core areas: vascularization and immune modulation. The vascular system is essential for bone regeneration, but current pre-vascularization strategies (such as co-printing endothelial cells or pre-fabricating perfusable channels) are still largely confined to *in vitro* stages. Rapid reconstruction of blood vessel networks and effective integration with the host vascular system post-implantation remain challenging, with common issues such as insufficient nutrient delivery, cell death, and delayed regeneration in the core regions of large-volume scaffolds. Delayed vascularization remains one of the major challenges limiting the clinical translation of large-volume bone constructs. At the same time, immune responses play a dual role in bone regeneration: moderate immune activation can promote

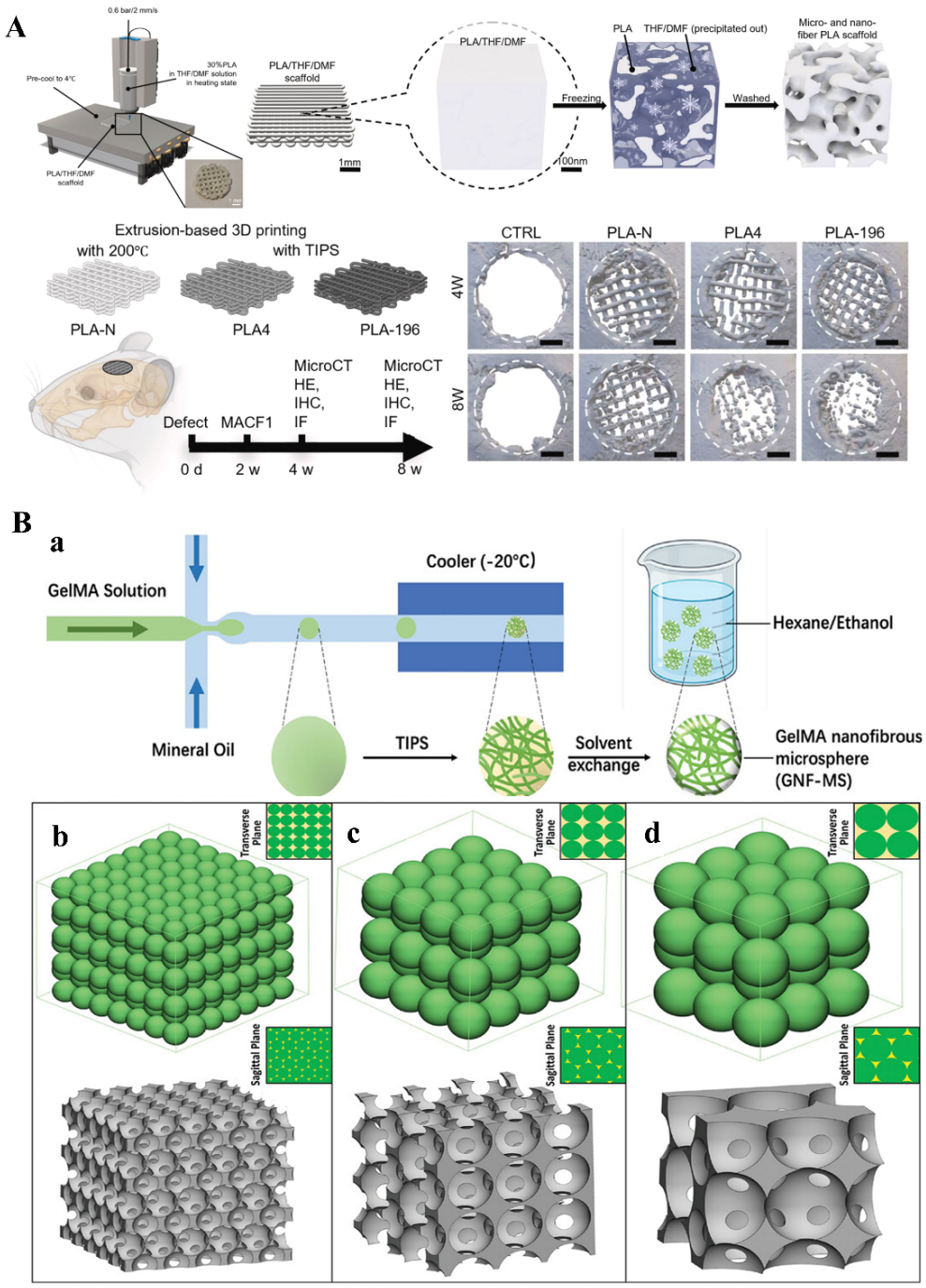


Figure 8. Nanoscale engineering integrated with 3D-printed bone scaffolds. (A) A hierarchical osteogenic PLA scaffold by 3D printing combined with thermally induced phase separation. Reprinted from Ref.[176] (B) 3D printing of a hierarchical porous nanofibrous scaffold for bone regeneration. (a) Schematic diagram of fabrication of GelMA nanofibrous microspheres. (b–d) 3D computer-simulated analysis diagrams of the local interstitial voids (second row) in regular and close-packed arrangement of uniform microspheres of different sizes (20, 33.3, and 50 μm), as well as the transverse and sagittal plane diagrams of the interstitial void distribution between microspheres (yellow). Reprinted with permission from Ref.[196] Copyright © 2024 Wiley-VCH GmbH.

Abbreviations: 3D: Three-dimensional; CTRL: Control; DMF: N,N-Dimethylformamide; GelMA: Gelatin methacryloyl; HE: Hematoxylin and eosin; IF: Immunofluorescence; IHC: Immunohistochemistry; MACF1: Microtubule-actin crosslinking factor 1; Micro-CT: Micro-computed tomography; PLA: Polylactic acid; THF: Tetrahydrofuran; TIPS: Thermally induced phase separation.

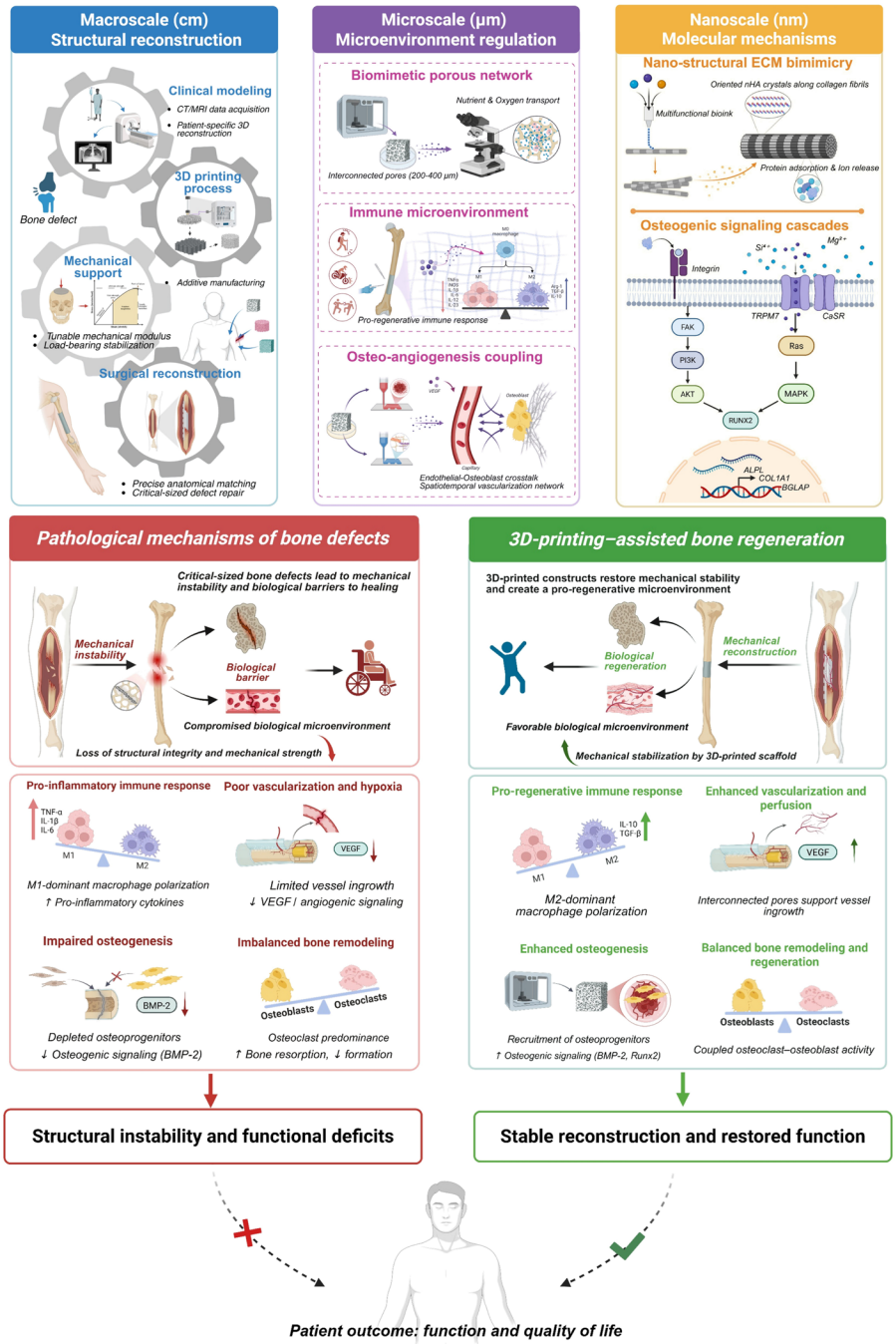


Figure 9. Macro–micro–nano multiscale design strategies and their roles in 3D printing-assisted bone regeneration. The schematic summarizes how multiscale 3D printing integrates structural reconstruction and biological regulation after bone injury. At the macroscale, patient-specific reconstruction restores anatomical geometry and mechanical stability. At the microscale, engineered pores, vascular networks, and immune-regulated microenvironments promote tissue integration. At the nanoscale, biomimetic interfaces and molecular signaling cues regulate cellular responses and osteogenic processes. The coordinated interaction among different scales contributes to stable and functional bone regeneration. Created in BioRender. Yang, W. (2026). https://BioRender.com/tyty4eo.

Abbreviations: 3D: Three-dimensional; AKT: Protein kinase B; ALPL: Alkaline phosphatase, biomineralization associated; BGLAP: Bone gamma-carboxyglutamate protein; BMP-2: Bone morphogenetic protein 2; CaSR: Calcium-sensing receptor; COL1A1: Collagen type I alpha 1 chain; CT: Computed tomography; ECM: Extracellular matrix; FAK: Focal adhesion kinase; HA: Hydroxyapatite; IL: Interleukin; MAPK: Mitogen-activated protein kinase; MRI: Magnetic resonance imaging; PI3K: Phosphoinositide 3-kinase; RUNX2: Runt-related transcription factor 2; TGF-β: Transforming growth factor beta; TNF-α: Tumor necrosis factor alpha; TRPM7: Transient receptor potential melastatin 7; VEGF: Vascular endothelial growth factor.

tissue repair, while excessive inflammation may trigger foreign body reactions, fibrosis, or even implant failure. Current research has paid insufficient attention to the immune microenvironment induced by scaffold materials, particularly in processes such as macrophage polarization (M1/M2 balance), T-cell responses, and immune-osteogenesis coupling. Future research must focus on how to achieve immunomodulatory bone regeneration through surface functionalization, topological optimization, or the incorporation of immune-modulatory factors.

Looking ahead, several emerging directions may further extend the functional scope of 3D-printed bone constructs. Four-dimensional printing introduces temporal responsiveness through shape-memory polymers or stimulus-responsive hydrogels, allowing scaffold geometry, mechanical properties, or therapeutic release to evolve during healing.[203] *In situ* bioprinting may provide another route toward patient-specific repair by depositing cell–material constructs directly at the defect site, although surgical integration and reproducibility remain major challenges. In parallel, osteoimmunology is becoming increasingly relevant to scaffold design, as material-induced immune responses can influence inflammation, vascularization, and subsequent bone formation. These developments broaden the role of 3D printing from static structural replacement toward dynamically regulated regeneration.

The integration of artificial intelligence and computational design is reshaping the development paradigm of multiscale 3D-printed bone scaffolds. At the application level, topology optimization algorithms have been employed to generate biomimetic scaffolds that simultaneously achieve high porosity and mechanical stability. For example, Laubach *et al.*[175] designed medical-grade PCL–HA scaffolds using a Voronoi-based algorithm, achieving uniform and tunable micro-porosity while maintaining macroscopic mechanical strength. Machine learning models are also used to predict scaffold mechanical properties and degradation behavior. Zarei *et al.*[204] provided a systematic review of additive manufacturing and machine learning strategies, highlighting that machine learning can analyze multiple parameters affecting scaffold performance—including pore size, porosity, surface roughness, and mechanical properties—and correlate these with *in vitro* and *in vivo* experimental results to develop predictive models that guide design and optimize scaffolds for enhanced bone regeneration. Furthermore, response surface methodology, as a classical experimental design tool, has been used by Thangavel *et al.*[83] to systematically optimize the filling ratio, sintering temperature, and material composition of WH/CS composite scaffolds, achieving multi-objective synergistic optimization. Nevertheless, current technical challenges include the high dimensionality of multiscale parameter spaces, which leaves available experimental datasets insufficient for robust model training, and the lack of effective integration of macroscopic, microscopic, and nanoscale physical models, limiting artificial intelligence predictions to single-scale optimization. Future directions should focus on developing hybrid frameworks combining physical modeling with machine learning, using finite element simulations to generate large-scale training datasets to compensate for limited experimental samples; advancing multiscale co-optimization algorithms that integrate macroscopic mechanics, microscopic mass transport, and nanoscale signaling as unified objectives; and promoting digital twin technologies throughout the scaffold lifecycle to achieve a predictive and controllable closed-loop system spanning design, printing, implantation, and degradation.

5. Conclusion

In conclusion, multiscale 3D printing for BTE should be viewed as the coordinated reconstruction of structural and biological functions across hierarchical levels rather than as the independent optimization of individual scales. At the macroscale, design should restore patient-specific anatomy and provide appropriate mechanical support and load transfer, which establishes the structural foundation for subsequent microscale biological organization. At the microscale, pore architecture, channels, and cellular organization should facilitate mass transport, vascular ingrowth, and spatial tissue formation while providing the local environment in which nanoscale biological cues operate. At the nanoscale, material interfaces and bioactive cues should regulate cell–material interactions and molecular signaling. The value of 3D printing lies in its ability to connect these requirements within a programmable manufacturing framework. Future progress will therefore depend less on maximizing structural complexity at any single scale than on achieving reproducible cross-scale coordination that supports stable, vascularized, and functionally integrated bone regeneration.

Acknowledgments

None.

Funding

This work was supported by the Innovation and Entrepreneurship Training Program for College Students in Henan Province (Grant No. S202510471035) and the Scientific Research Seedling Engineering of Henan University of Chinese Medicine (Grant Nos. 2025MPXS18 and 2025MPXS25).

Conflict of interest

The authors declare they have no competing interests.

Author contributions

Conceptualization: Pengbei Fan, Lin Zhu, Yujie Wang
Supervision: Pengbei Fan, Lin Zhu, Yujie Wang
Visualization: Maisha Feng, Yue Wang, Li Ji, Jinfan Wei, Linyi Wang, Yueyang Wang
Writing–original draft: Yueyang Wang, Yazhe Fan
Writing–review & editing: Pengbei Fan, Lin Zhu, Yujie Wang

Ethics approval and consent to participate

Not applicable.

Consent for publication

Not applicable.

Availability of data

Not applicable.

References

1. Wang Y-x, Deng Z-h, Li Y-y, *et al*. Function of hematopoiesis and bone marrow niche in inflammation and non-hematopoietic diseases. *Life Med*. 2025;4(3):lnaf015.

   doi: 10.1093/lifemedi/lnaf015

2. Wu A-M, Bisignano C, James SL, *et al*. Global, regional, and national burden of bone fractures in 204 countries and territories, 1990–2019: a systematic analysis from the Global Burden of Disease Study 2019. *Lancet Healthy Longev*. 2021;2(9):e580-e592.

   doi: 10.1016/S2666-7568(21)00172-0

3. Yue X, Sun X, Li Z, *et al*. Biomimetic Piezoelectric Periosteum-Bone Integrated Implant Promotes Bone Defect Repair by Remodeling Osteogenic Microenvironment. *Adv Funct Mater*. 2025;35(35):2423492.

   doi: 10.1002/adfm.202423492

4. Gläser N, Schröder M, Barcik J, Haffner-Luntzer M, Wehrle E. Extended view on the mechanobiology of fracture healing: interplay between mechanics and inflammation. *Front Bioeng Biotechnol*. 2025;13:1652897.

   doi: 10.3389/fbioe.2025.1652897

5. Steppe L, Megafu M, Tschaffon-Müller MEA, Ignatius A, Haffner-Luntzer M. Fracture healing research: Recent insights. *Bone Rep*. 2023;19:101686.

   doi: 10.1016/j.bonr.2023.101686

6. Moghaddam A, Bahrami M, Mirzadeh M, *et al*. Recent trends in bone tissue engineering: a review of materials, methods, and structures. *Biomed Mater*. 2024;19(4):042007.

   doi: 10.1088/1748-605X/ad407d

7. Laubach M, Whyte S, Chan HF, *et al*. Lost in translation: the lack of agreement between surgeons and scientists regarding biomaterials research and innovation for treating bone defects. *BMC Med*. 2024;22(1):517.

   doi: 10.1186/s12916-024-03734-z

8. Fernandez de Grado G, Keller L, Idoux-Gillet Y, *et al*. Bone substitutes: a review of their characteristics, clinical use, and perspectives for large bone defects management. *J Tissue Eng*. 2018;9:2041731418776819.

   doi: 10.1177/2041731418776819

9. Santoro A, Voto A, Fortino L, *et al*. Bone defect treatment in regenerative medicine: exploring natural and synthetic bone substitutes. *Int J Mol Sci*. 2025;26(7):3085.

   doi: 10.3390/ijms26073085

10. Ivanova N, Ivanov S, Peev S, Dikova T. Types of bone substitutes and their application in regenerative medicine: A systematic review. *J Funct Biomater*. 2025;16(9):341.

    doi: 10.3390/jfb16090341

11. Huang L, Guo Z, Yang X, *et al*. Advancements in GelMA bioactive hydrogels: Strategies for infection control and bone tissue regeneration. *Theranostics*. 2025;15(2):460-493.

    doi: 10.7150/thno.103725

12. Ngo TD, Kashani A, Imbalzano G, Nguyen KTQ, Hui D. Additive manufacturing (3D printing): A review of materials, methods, applications and challenges. *Compos B Eng*. 2018;143:172-196.

    doi: 10.1016/j.compositesb.2018.02.012

13. Bose S, Vahabzadeh S, Bandyopadhyay A. Bone tissue engineering using 3D printing. *Mater Today*. 2013;16(12):496-504.

    doi: 10.1016/j.mattod.2013.11.017

14. Sun J, Chen C, Zhang B, Yao C, Zhang Y. Advances in 3D-printed scaffold technologies for bone defect repair: materials, biomechanics, and clinical prospects. *Biomed Eng Online*. 2025;24(1):51.

    doi: 10.1186/s12938-025-01381-w

15. Zhou J, See CW, Sreenivasamurthy S, Zhu D. Customized additive manufacturing in bone scaffolds—the gateway to precise bone defect treatment. *Research*. 2023;6:0239.

    doi: 10.34133/research.0239

16. Luo Q, Shang K, Zhu J, *et al*. Biomimetic cell culture for cell adhesive propagation for tissue engineering strategies. *Mater Horiz*. 2023;10(11):4662-4685.

    doi: 10.1039/d3mh00849e

17. Singaravelu S, Abrahamse H, Kumar SSD. Three-dimensional bio-derived materials for biomedical applications: challenges and opportunities. *RSC Adv*. 2025;15(12):9375-9397.

doi: 10.1039/d4ra07531e

18. Hull CW. Apparatus for production of three-dimensional objects by stereolithography. United States patent 4,575,330. March 11, 1986.

19. Deckard CR, Beaman JJ. Solid freeform fabrication and selective powder sintering. In: *Proceedings of the 15th North American Manufacturing Research Conference*; 1987:636-640.

20. Crump S. The extrusion process of fused deposition modeling. In: *Proceedings of the 3rd International Conference on Rapid Prototyping*. June 7–10, 1992; Dayton, OH. pp. 91–102.

21. Lin S, German R. Interaction between binder and powder in injection moulding of alumina. *J Mater Sci*. 1994;29(19):5207-5212.

doi: 10.1007/BF01151118

22. Hutmacher DW, Schantz T, Zein I, Ng KW, Teoh SH, Tan KC. Mechanical properties and cell cultural response of polycaprolactone scaffolds designed and fabricated via fused deposition modeling. *J Biomed Mater Res*. 2001;55(2):203-216.

doi: 10.1002/1097-4636(200105)55:2<203::aid-jbm1007>3.0.co;2-7

23. Anada T, Pan C-C, Stahl AM, *et al*. Vascularized bone-mimetic hydrogel constructs by 3D bioprinting to promote osteogenesis and angiogenesis. *Int J Mol Sci*. 2019;20(5):1096.

doi: 10.3390/ijms20051096

24. Chiesa I, De Maria C, Lapomarda A, *et al*. Endothelial cells support osteogenesis in an in vitro vascularized bone model developed by 3D bioprinting. *Biofabrication*. 2020;12(2):025013.

doi: 10.1088/1758-5090/ab6a1d

25. Shen M, Wang L, Gao Y, *et al*. 3D bioprinting of in situ vascularized tissue engineered bone for repairing large segmental bone defects. *Mater Today Bio*. 2022;16:100382.

doi: 10.1016/j.mtbio.2022.100382

26. Gong M, Zha Y, Lu S, *et al*. Efficacy and safety of the low-temperature-derived 3D printed biodegradable Mg-containing composite porous scaffold for bone defect repair: A prospective and multi-center randomized controlled trial. *Biomaterials*. 2026;327:123751.

doi: 10.1016/j.biomaterials.2025.123751

27. Kumar P, Sharma J, Kumar R, *et al*. Advances in bioink-based 3D printed scaffolds: optimizing biocompatibility and mechanical properties for bone regeneration. *Biomater Sci*. 2025;13(10):2556-2579.

doi: 10.1039/D4BM01606H

28. Zou R, Han X, Meng Y, *et al*. Improved mechanical performance and forming accuracy of ZrO2 fixed partial denture based on the digital light processing technology. *J Mech Behav Biomed Mater*. 2025;163:106840.

doi: 10.1016/j.jmbbm.2024.106840

29. Sarraf M, Rezvani Ghomi E, Alipour S, Ramakrishna S, Liana Sukiman N. A state-of-the-art review of the fabrication and characteristics of titanium and its alloys for biomedical applications. *Bio-Des Manuf*. 2022;5(2):371-395.

doi: 10.1007/s42242-021-00170-3

30. Sivasankar MV, Chinta ML, Sreenivasa Rao P. Zirconia based composite scaffolds and their application in bone tissue engineering. *Int J Biol Macromol*. 2024;265:130558.

doi: 10.1016/j.ijbiomac.2024.130558

31. Maté-Sánchez de Val JE, Mazón P, Calvo-Guirado JL, *et al*. Comparison of three hydroxyapatite/β-tricalcium phosphate/collagen ceramic scaffolds: An in vivo study. *J Biomed Mater Res A*. 2014;102(4):1037-1046.

doi: 10.1002/jbm.a.34785

32. Jensen SS, Yeo A, Dard M, Hunziker E, Schenk R, Buser D. Evaluation of a novel biphasic calcium phosphate in standardized bone defects. A histologic and histomorphometric study in the mandibles of minipigs. *Clin Oral Implants Res*. 2007;18(6):752-760.

doi: 10.1111/j.1600-0501.2007.01417.x

33. Jeong J, Kim JH, Shim JH, Hwang NS, Heo CY. Bioactive calcium phosphate materials and applications in bone regeneration. *Biomater Res*. 2019;23:4.

doi: 10.1186/s40824-018-0149-3

34. Cui J, Xia L, Lin K, Wang X. In situ construction of a nano-structured akermanite coating for promoting bone formation and osseointegration of Ti–6Al–4V implants in a rabbit osteoporosis model. *J Mater Chem B*. 2021;9(46):9505-9513.

doi: 10.1039/d1tb01917a

35. Liu K, Wang J, Fang S, *et al*. Effect of polycaprolactone impregnation on the properties of calcium silicate scaffolds fabricated by 3D printing. *Mater Des*. 2022;220:110856.

doi: 10.1016/j.matdes.2022.110856

36. Wu C, Chang J, Zhai W, Ni S, Wang J. Porous akermanite scaffolds for bone tissue engineering: Preparation, characterization, and in vitro studies. *J Biomed Mater Res B Appl Biomater*. 2006;78(1):47-55.

doi: 10.1002/jbm.b.30456

37. Niinomi M, Liu Y, Nakai M, Liu H, Li H. Biomedical titanium alloys with Young's moduli close to that of cortical bone. *Regen Biomater*. 2016;3(3):173-185.

doi: 10.1093/rb/rbw016

38. Yao B, Liu Z, Li H, *et al*. Research on SLM formation and fatigue properties of Ti6Al4V femoral porous structures

based on topology optimization. *Mater Chem Phys*. 2025;347:131484.

doi: 10.1016/j.matchemphys.2025.131484

39. Ceddia M, Romasco T, Pietro ND, *et al*. Quantifying Stress Shielding in Dental Implants: A Comparative Finite Element Study of Titanium, CFR-PEEK, and Ceramic Materials. *Materials*. 2026;19(5):869.

doi: 10.3390/ma19050869

40. Wang L, Wang X, Wu J, *et al*. Magnesium Ions Induce Endothelial Cell Differentiation into Tip Cell and Enhance Vascularized Bone Regeneration. *Adv Healthcare Mater*. 2025;14(19):e2500274.

doi: 10.1002/adhm.202500274

41. Drotárová L, Slámečka K, Balint T, *et al*. Biodegradable WE43 Mg alloy/hydroxyapatite interpenetrating phase composites with reduced hydrogen evolution. *Bioact Mater*. 2024;42:519-530.

doi: 10.1016/j.bioactmat.2024.08.048

42. Li D, Zhang D, Yuan Q, *et al*. In vitro and in vivo assessment of the effect of biodegradable magnesium alloys on osteogenesis. *Acta Biomater*. 2022;141:454-465.

doi: 10.1016/j.actbio.2021.12.032

43. Ma H, Wu L, Liu C, *et al*. First-principles modeling of the hydrogen evolution reaction and its application in electrochemical corrosion of Mg. *Acta Mater*. 2020;183:377-389.

doi: 10.1016/j.actamat.2019.11.025

44. Li P, Dai J, Li Y, *et al*. Zinc based biodegradable metals for bone repair and regeneration: Bioactivity and molecular mechanisms. *Mater Today Bio*. 2024;25:100932.

doi: 10.1016/j.mtbio.2023.100932

45. Yang X, Peng Z, Fang Y, Tang Y, Shen H-H, Zhu Y. Review of additively manufactured zinc alloys by laser powder bed fusion for biomedical applications. *Rare Met*. 2025;44(11):8262-8291.

doi: 10.1007/s12598-025-03518-1

46. Wang X, Liu A, Zhang Z, *et al*. Additively Manufactured Zn-2Mg Alloy Porous Scaffolds with Customizable Biodegradable Performance and Enhanced Osteogenic Ability. *Adv Sci*. 2024;11(5):2307329.

doi: 10.1002/advs.202307329

47. Dong Z, Han C, Liu G, *et al*. Revealing anisotropic mechanisms in mechanical and degradation properties of zinc fabricated by laser powder bed fusion additive manufacturing. *J Mater Sci Technol*. 2025;214:87-104.

doi: 10.1016/j.jmst.2024.06.045

48. Jiao J, Hong Q, Zhang D, *et al*. Influence of porosity on osteogenesis, bone growth and osteointegration in trabecular tantalum scaffolds fabricated by additive manufacturing. *Front Bioeng Biotechnol*. 2023;11:1117954.

doi: 10.3389/fbioe.2023.1117954

49. Wang X, Liu W, Jiang C, *et al*. Research progress on the osteogenic properties of tantalum in the field of medical implant materials. *J Mater Res Technol*. 2024;30:1706-1715.

doi: 10.1016/j.jmrt.2024.03.200

50. Bobyn JD, Stackpool GJ, Hacking SA, Tanzer M, Krygier JJ. Characteristics of bone ingrowth and interface mechanics of a new porous tantalum biomaterial. *J Bone Joint Surg Br*. 1999;81-B(5):907-914.

doi: 10.1302/0301-620x.81b5.0810907

51. Choi Y, Kim C, Kim HS, Moon C, Lee KY. 3D Printing of dynamic tissue scaffold by combining self-healing hydrogel and self-healing ferrogel. *Colloids Surf, B*. 2021;208:112108.

doi: 10.1016/j.colsurfb.2021.112108

52. Amini-Mosleh-Abadi S, Yazdanpanah Z, Ketabat F, *et al*. In vitro characterization of 3D printed polycaprolactone/graphene oxide scaffolds impregnated with alginate and gelatin hydrogels for bone tissue engineering. *J Biomater Appl*. 2025;40(3):374-388.

doi: 10.1177/08853282251336552

53. Guo L, Liang Z, Yang L, *et al*. The role of natural polymers in bone tissue engineering. *J Controlled Release*. 2021;338:571-582.

doi: 10.1016/j.jconrel.2021.08.055

54. Yang XB, Roach HI, Clarke NMP, *et al*. Human osteoprogenitor growth and differentiation on synthetic biodegradable structures after surface modification. *Bone*. 2001;29(6):523-531.

doi: 10.1016/s8756-3282(01)00617-2

55. Takagi A, Hsu Y-I, Uyama H. Biodegradable poly (lactic acid) and polycaprolactone alternating multiblock copolymers with controllable mechanical properties. *Polym Degrad Stab*. 2023;218:110564.

doi: 10.1016/j.polymdegradstab.2023.110564

56. Zhu S, Sun H, Mu T, Richel A. Research Progress in 3D Printed Biobased and Biodegradable Polyester/Ceramic Composite Materials: Applications and Challenges in Bone Tissue Engineering. *ACS Appl Mater Interfaces*. 2025;17(2):2791-2813.

doi: 10.1021/acsami.4c15719

57. Shirali D, Emadi R, Khodaei M, Emadi H, Arab Eshagh Abadi M, Tayebi L. Surface modification of 3D-printed polylactic acid-hardystonite scaffold for bone tissue engineering. *Int J Biol Macromol*. 2025;308:142496.

doi: 10.1016/j.ijbiomac.2025.142496

58. Mathur V, Agarwal P, Kasturi M, Srinivasan V, Seetharam

RN, Vasanthan KS. Innovative bioinks for 3D bioprinting: Exploring technological potential and regulatory challenges. *J Tissue Eng*. 2025;16:20417314241308022.

doi: 10.1177/20417314241308022

59. Singh AK, Pramanik K, Biswas A. Constructing a biofunctionalized 3D-printed gelatin/sodium alginate/chitosan tri-polymer complex scaffold with improvised biological and mechanical properties for bone-tissue engineering. *Bio-Des Manuf*. 2024;7(1):57-73.

doi: 10.1007/s42242-023-00249-z

60. Aminmansour S, Cardoso LM, Anselmi C, de Carvalho ABG, Rahimnejad M, Bottino MC. Development of Cerium Oxide-Laden GelMA/PCL Scaffolds for Periodontal Tissue Engineering. *Materials*. 2024;17(16):3904.

doi: 10.3390/ma17163904

61. Li D, Chen P, Du H, Li Z, Li M, Xu Y. 3D-Printed Shape Memory and Piezoelectric Bifunctional Thermoplastic Polyurethane/Polyvinylidene Fluoride Porous Composite Scaffold for Bone Regeneration. *ACS Biomater Sci Eng*. 2024;10(11):7100-7110.

doi: 10.1021/acsbiomaterials.4c01221

62. Li Z, Li G, Wang X, Zhao Z. Piezoelectric composite hydrogel with wireless electrical stimulation enhances motor functional recovery of spinal cord injury. *J Mater Sci Technol*. 2024;172:228-239.

doi: 10.1016/j.jmst.2023.07.014

63. Liu J, Han Y, Hu C, Wang Y, He C. The Evolution and Frontiers of Piezoelectric Materials for Bone and Cartilage Regeneration Research. *Tissue Eng Part C Methods*. 2025;31(12):396-414.

doi: 10.1177/19373384251405475

64. Zheng H, Yan P, Liu P, *et al*. Ultrasound-activated piezoelectric scaffolds target dual Ca2+/NF-κB signaling pathways to orchestrate immunomodulation and osteogenesis for accelerated bone regeneration. *Mater Today Bio*. 2025;35:102299.

doi: 10.1016/j.mtbio.2025.102299

65. Huang H, Wang K, Liu X, *et al*. Piezoelectric biomaterials for providing electrical stimulation in bone tissue engineering: Barium titanate. *J Orthop Translat*. 2025;51:94-107.

doi: 10.1016/j.jot.2024.12.011

66. Zhang C, Cai D, Liao P, *et al*. 4D Printing of shape-memory polymeric scaffolds for adaptive biomedical implantation. *Acta Biomater*. 2021;122:101-110.

doi: 10.1016/j.actbio.2020.12.042

67. Mahjoubnia A, Cai D, Wu Y, *et al*. Digital light 4D printing of bioresorbable shape memory elastomers for personalized biomedical implantation. *Acta Biomater*. 2024;177:165-177.

doi: 10.1016/j.actbio.2024.02.009

68. Hu X, He J, Yong X, *et al*. Biodegradable poly (lactic acid-co-trimethylene carbonate)/chitosan microsphere scaffold with shape-memory effect for bone tissue engineering. *Colloids Surf B*. 2020;195:111218.

doi: 10.1016/j.colsurfb.2020.111218

69. Li B, Ma Y, Fatima K, *et al*. 3D printed shape-memory piezoelectric scaffolds with in-situ self-power properties for bone defect repair. *J Nanobiotechnol*. 2025;23(1):244.

doi: 10.1186/s12951-025-03325-x

70. Liu C, Xie Y, Zhang Y, *et al*. MOF-Based Guided Bone Regeneration Membrane for Promoting Osteogenesis by Regulating Bone Microenvironment through Cascade Effects. *Adv Healthcare Mater*. 2024;14(26):e2403187.

doi: 10.1002/adhm.202403187

71. Liu X, Schreiber AC, Astudillo Potes MD, *et al*. Bone Enzyme-Responsive Biodegradable Poly(propylene fumarate) and Polycaprolactone Polyphosphoester Dendrimer Cross-Linked via Click Chemistry for Bone Tissue Engineering. *Biomacromolecules*. 2025;26(2):835-847.

doi: 10.1021/acs.biomac.4c00999

72. Fu X, Luo Z, Guo Y, *et al*. Microenvironment-responsive multifunctional enzyme-linked hydrogel for diabetic bone defect regeneration. *Nat Commun*. 2025;16(1):10275.

doi: 10.1038/s41467-025-65165-5

73. Liu H, Ai R, Liu B, He L. Dual ROS/Glucose-Responsive Quercetin-Loaded Supramolecular Hydrogel for Diabetic Wound Healing. *Biomacromolecules*. 2025;26(3):1541-1554.

doi: 10.1021/acs.biomac.4c01331

74. Wei H, Cui J, Lin K, Xie J, Wang X. Recent advances in smart stimuli-responsive biomaterials for bone therapeutics and regeneration. *Bone Res*. 2022;10(1):17.

doi: 10.1038/s41413-021-00180-y

75. Chen F, Zhu H, Wu J-M, *et al*. Preparation and biological evaluation of ZrO2 all-ceramic teeth by DLP technology. *Ceram Int*. 2020;46(8):11268-11274.

doi: 10.1016/j.ceramint.2020.01.152

76. Zhao X, Liu J, Li L. Research Progress and Challenges in 3D Printing of Bioceramics and Bioceramic Matrix Composites. *Biomimetics*. 2025;10(7):428.

doi: 10.3390/biomimetics10070428

77. Zhang H, Jiao C, He Z, *et al*. Fabrication and properties of 3D printed zirconia scaffold coated with calcium silicate/hydroxyapatite. *Ceram Int*. 2021;47(19):27032-27041.

doi: 10.1016/j.ceramint.2021.06.116

78. Ma H, Feng C, Chang J, Wu C. 3D-printed bioceramic scaffolds: From bone tissue engineering to tumor

therapy. *Acta Biomater*. 2018;79:37-59.

doi: 10.1016/j.actbio.2018.08.026

79. Xu C, Wu F, Yang J, *et al*. 3D printed long-term structurally stable bioceramic dome scaffolds with controllable biodegradation favorable for guided bone regeneration. *Chem Eng J*. 2022;450:138003.

doi: 10.1016/j.cej.2022.138003

80. Liu R, Ma L, Liu H, Xu B, Feng C, He R. Effects of pore size on the mechanical and biological properties of stereolithographic 3D printed HAp bioceramic scaffold. *Ceram Int*. 2021;47(20):28924-28931.

doi: 10.1016/j.ceramint.2021.07.053

81. Sarode B, Kuthe A, Bhishnurkar AD, Bagde AD. Influence of heating rate and soak time on microwave sintered hydroxyapatite and β-tricalcium phosphate ceramics for bone applications. *Sci Rep*. 2026;16(1):1182.

doi: 10.1038/s41598-025-30915-4

82. Kim H-W, Lee H-H, Chun G-S. Bioactivity and osteoblast responses of novel biomedical nanocomposites of bioactive glass nanofiber filled poly(lactic acid). *J Biomed Mater Res Part A*. 2008;85A(3):651-663.

doi: 10.1002/jbm.a.31339

83. Thangavel M, Elsen SR. Evaluation and optimization of physical, mechanical, and biological characteristics of 3D printed Whitlockite/calcium silicate composite scaffold for bone tissue regeneration using response surface methodology. *Biomed Mater*. 2025;20(2):025017.

doi: 10.1088/1748-605X/adad27

84. Zhu W, Zhao T, Wang H, *et al*. Injectable and Assembled Calcium Sulfate/Magnesium Silicate 3D Scaffold Promotes Bone Repair by In Situ Osteoinduction. *Bioengineering*. 2025;12(6):599.

doi: 10.3390/bioengineering12060599

85. Shearer A, Montazerian M, Mauro JC. Modern definition of bioactive glasses and glass-ceramics. *J Non-Cryst Solids*. 2023;608:122228.

doi: 10.1016/j.jnoncrysol.2023.122228

86. Shendage SS, Kamble G, Chavan R, *et al*. Bioactive Glass for Bone Tissue Regeneration: Focusing on the Key Biological Properties. *ACS Biomater Sci Eng*. 2026;12(1):71-89.

doi: 10.1021/acsbiomaterials.5c01283

87. Li S, Mohammed AA, Nommeots-Nomm A, *et al*. Human bone marrow derived stem cell differentiation on 3D printed bioactive glass scaffolds. *J Mater Sci Mater Med*. 2025;36(1):69.

doi: 10.1007/s10856-025-06918-y

88. Lee CY, Kung PC, Huang CC, *et al*. In Vivo Study of Bone Growth Around Additively Manufactured Implants With Ti-6Al-4V and Bioactive Glass Powder Composites. *J Orthop Res*. 2025;43(10):1796-1804.

doi: 10.1002/jor.70037

89. Zhang X, Zu H, Zhao D, *et al*. Ion channel functional protein kinase TRPM7 regulates Mg ions to promote the osteoinduction of human osteoblast via PI3K pathway: In vitro simulation of the bone-repairing effect of Mg-based alloy implant. *Acta Biomater*. 2017;63:369-382.

doi: 10.1016/j.actbio.2017.08.051

90. Sheng X, Li C, Wang Z, *et al*. Advanced applications of strontium-containing biomaterials in bone tissue engineering. *Mater Today Bio*. 2023;20:100636.

doi: 10.1016/j.mtbio.2023.100636

91. Shan Y, Bai Y, Zhao L, *et al*. Three-dimensional-printed strontium-incorporated β-TCP bioceramic triply periodic minimal surface scaffolds with enhanced angiogenic and osteogenic properties. *Regen Biomater*. 2025;12:rbaf080.

doi: 10.1093/rb/rbaf080

92. Deng F, Bu Z, Hu H, Huang X, Liu Z, Ning C. Bioadaptable bone regeneration of Zn-containing silicocarnotite bioceramics with moderate biodegradation and antibacterial activity. *Appl Mater Today*. 2022;27:101433.

doi: 10.1016/j.apmt.2022.101433

93. Fan Y, Yao J, Liu W, *et al*. 3D printed composite scaffold accelerates bone regeneration by modulating immunity and promoting angiogenesis. *J Mater Sci Technol*. 2026;240:1-18.

doi: 10.1016/j.jmst.2025.03.041

94. Ho C-C, Hsu T-T, Chiu Y-C, Lin Y-H, Xie P-C, Wang C-Y. 3D-printed magnesium/strontium-co-doped calcium silicate scaffolds promote angiogenesis and bone regeneration through synergistic bioactive ion stimulation. *J Biol Eng*. 2025;19(1):58.

doi: 10.1186/s13036-025-00528-6

95. Chen L, Zhou C, Xie Q, *et al*. Zinc Doped Synthetic Polymer Composites for Bone Regeneration: A Promising Strategy to Repair Bone Defects. *Int J Nanomed*. 2025;20:8567-8586.

doi: 10.2147/IJN.S512994

96. Sharma D, Nouri A, Sharma V. Strategic Control of Porosity and Post-Processing in Additive Manufacturing of Metallic Bone Scaffolds. *Adv Eng Mater*. 2025;27(17):2500749.

doi: 10.1002/adem.202500749

97. Wang X, Liu W, Yu X, *et al*. Advances in surface modification of tantalum and porous tantalum for rapid osseointegration: A thematic review. *Front Bioeng Biotechnol*. 2022;10:983695.

doi: 10.3389/fbioe.2022.983695

98. Gokyer S, Monsef YA, Buyuksungur S, *et al*. MgCa-Based Alloys Modified with Zn- and Ga-Doped CaP Coatings Lead to Controlled Degradation and Enhanced Bone Formation

in a Sheep Cranium Defect Model. *ACS Biomater Sci Eng*. 2024;10(7):4452-4462.

doi: 10.1021/acsbiomaterials.4c00358

99. Goto M, Matsumine A, Yamaguchi S, *et al*. Osteoconductivity of bioactive Ti-6Al-4V implants with lattice-shaped interconnected large pores fabricated by electron beam melting. *J Biomater Appl*. 2021;35(9):1153-1167.

doi: 10.1177/0885328220968218

100. Li D, Xie H, Gao C, Jiang H, Wang L, Shuai C. Harmonic heterostructured pure Ti fabricated by laser powder bed fusion for excellent wear resistance via strength-plasticity synergy. *Opto-Electron Adv*. 2025;8(9):250043.

doi: 10.29026/oea.2025.250043

101. Abd-Elaziem W, Darwish MA, Hamada A, Daoush WM. Titanium-Based alloys and composites for orthopedic implants Applications: A comprehensive review. *Mater Des*. 2024;241:112850.

doi: 10.1016/j.matdes.2024.112850

102. Dhinasekaran D, Sivakumar JP, Rajendran AR. Enhancement of implant performance through synergistic drug delivery and bioactivity by nanotubular titanium with hydroxyapatite coating. *Int J Pharm*. 2025;681:125854.

doi: 10.1016/j.ijpharm.2025.125854

103. Xu D, Wang X, Li M, *et al*. Enhancing titanium-osteointegration: antimicrobial, anti-inflammatory and osteogenic properties of multifunctional coatings through layer-by-layer self-assembly. *Appl Surf Sci*. 2025;686:162149.

doi: 10.1016/j.apsusc.2024.162149

104. Nezhad AN, Zahrani EM, Mousavinasab S, Alfantazi A. A comprehensive review of additively manufactured biomedical titanium alloys for bone tissue engineering: Biocorrosion, biomechanical, and biological properties. *J Mater Res Technol*. 2025;36:9113-9157.

doi: 10.1016/j.jmrt.2025.05.069

105. Hashmi AW, Tian Y, Wang C, *et al*. Adapted interfaces in magnesium alloys for biomedical applications: Synthesis, properties, and performance enhancement. *J Alloys Compd*. 2025;1048:185179.

doi: 10.1016/j.jallcom.2025.185179

106. Aikin M, Shalomeev V, Kukhar V, *et al*. Recent advances in biodegradable magnesium alloys for medical implants: evolution, innovations, and clinical translation. *Crystals*. 2025;15(8):671.

doi: 10.3390/cryst15080671

107. Raj V, Sabarinath S, Vignesh RV, Padil VV. Structure–Property–Biocompatibility Interplay in Heat-Treated WE43 Magnesium Alloy. *Mater Chem Phys*. 2025;348(2):131623.

doi: 10.1016/j.matchemphys.2025.131623

108. Dong L, Zhang G, Shen Z, *et al*. Degradation of WE43 Magnesium Alloy in Vivo and Its Degradation Products on Macrophages. *ACS Omega*. 2025;10(17):17280-17295.

doi: 10.1021/acsomega.4c09349

109. Yang H, Huang H, Li S, *et al*. Biodegradable zinc-based metallic materials: Mechanisms, properties, and applications. *Prog Mater Sci*. 2026;157:101584.

doi: 10.1016/j.pmatsci.2025.101584

110. Liang S, Du S, Zheng Y, Xia D, Zhou Y. Biodegradable Zn-xY alloys with enhanced osteogenesis and angiogenesis effects for bone implant applications. *Acta Biomater*. 2025;201:684-702.

doi: 10.1016/j.actbio.2025.05.048

111. Wang X, Xu S, Zhou S, *et al*. Topological design and additive manufacturing of porous metals for bone scaffolds and orthopaedic implants: A review. *Biomaterials*. 2016;83:127-141.

doi: 10.1016/j.biomaterials.2016.01.012

112. Liu A, Wang C, Zhao Z, *et al*. Progress of porous tantalum surface-modified biomaterial coatings in bone tissue engineering. *J Mater Sci Mater Med*. 2025;36(1):26.

doi: 10.1007/s10856-025-06871-w

113. Wauthle R, Van der Stok J, Yavari SA, *et al*. Additively manufactured porous tantalum implants. *Acta Biomater*. 2015;14:217-225.

doi: 10.1016/j.actbio.2014.12.003

114. Ilo KC, Van Duren BH, Berber R, Matar HE, Manktelow AR, Bloch BV. Comparing trabecular metal versus fiber mesh cementless acetabular components: a single-center study of 6,563 hips. *J Arthroplasty*. 2025;40(6):1589-1593.

doi: 10.1016/j.arth.2024.11.048

115. Tang H, Yang K, Jia L, He W, Yang L, Zhang X. Tantalum Bone Implants Printed by Selective Electron Beam Manufacturing (SEBM) and Their Clinical Applications. *JOM*. 2020;72(3):1016-1021.

doi: 10.1007/s11837-020-04016-8

116. Srinivasan S, Vijayalekha A, Pandurangan AK. Eugenol-loaded sodium Alginate/Chitosan/β-TCP composite scaffold for bone defect regeneration: an in-silico and in-vitro evaluation. *Biotechnol Sustain Mater*. 2025;2(1):25.

doi: 10.1186/s44316-025-00048-9

117. Zhu Y, Yu X, Liu H, *et al*. Strategies of functionalized GelMA-based bioinks for bone regeneration: recent advances and future perspectives. *Bioact Mater*. 2024;38:346-373.

doi: 10.1016/j.bioactmat.2024.04.032

118. Gharibshahian M, Salehi M, Beheshtizadeh N, *et al*. Recent advances on 3D-printed PCL-based composite scaffolds for bone tissue engineering. *Front Bioeng Biotechnol*.

2023;11:1168504.

doi: 10.3389/fbioe.2023.1168504

119. Chen Y, Zhang G, Ge D, Wang M, Wu T, Zou Z. Physicochemical properties and biocompatibility of 3D printed PVDF-TrFE-CPS composite bone scaffolds with piezoelectric properties. *Mater Des*. 2025;260:115004.

doi: 10.1016/j.matdes.2025.115004

120. Meng D, Hou Y, Zubairi H, *et al*. Ceramic-based piezoelectric material reinforced 3D printed polycaprolactone bone tissue engineering scaffolds. *Mater Des*. 2025;257:114542.

doi: 10.1016/j.matdes.2025.114542

121. Dixon DT, Landree EN, Gomillion CT. Biomimetic Dual-Sensing Bone Scaffolds: Characterization and In Vitro Evaluation Under Dynamic Culturing Conditions. *Biomimetics*. 2025;10(9):598.

doi: 10.3390/biomimetics10090598

122. Wang Y, Zhang H, Xu Z, *et al*. Icariin-loaded GelMa hydrogel encapsulated potassium sodium niobate biomimetic piezoelectric scaffold regulates macrophage polarization to accelerate bone defect repair. *Mater Today Bio*. 2025;35:102476.

doi: 10.1016/j.mtbio.2025.102476

123. Yang S, Hu Q, Hu Y, *et al*. Sequential treatment of infectious bone defects with 3D-printed body temperature-responsive shape memory scaffold coated with metal-polyphenol layers. *Burns Trauma*. 2026;14:tkaf072.

doi: 10.1093/burnst/tkaf072

124. Lv S, Zhang Y, Liang X, *et al*. Biomimetic Barium Titanate/PLA Scaffold with Shape Memory and Bioelectro-Active Capacities Promotes Bone Regeneration. *Int J Nanomed*. 2025;20:13231-13253.

doi: 10.2147/IJN.S524080

125. Chen S, Zhou X, Wang X, Li H, An R, Qian Y. Magnetical scafford with ROS-scavenging for bone regeneration under static magnetic field. *Colloids Surf B*. 2025;245:114245.

doi: 10.1016/j.colsurfb.2024.114245

126. Kumar P, Shamim, Muztaba M, *et al*. Fused Deposition Modeling 3D-Printed Scaffolds for Bone Tissue Engineering Applications: A Review. *Ann Biomed Eng*. 2024;52(5):1184-1194.

doi: 10.1007/s10439-024-03479-z

127. Wu B, Yang J, Ye J, *et al*. Extrusion-based 3D printing of cross-scale porous bone scaffolds and their micro-topological structures for bone repair. *Biomater Adv*. 2026;180:214540.

doi: 10.1016/j.bioadv.2025.214540

128. Manzoli S, Merotto E, Piccoli M, Gobbo P, Todros S, Pavan PG. An Overview of 3D Bioprinting Impact on Cell Viability: From Damage Assessment to Protection Solutions. *J Funct Biomater*. 2025;16(12):436.

doi: 10.3390/jfb16120436

129. Yogeshwaran S, Goodarzi Hosseinabadi H, Gendy DE, Miri AK. Design considerations and biomaterials selection in embedded extrusion 3D bioprinting. *Biomater Sci*. 2024;12(18):4506-4518.

doi: 10.1039/d4bm00550c

130. Hinton TJ, Jallerat Q, Palchesko RN, *et al*. Three-dimensional printing of complex biological structures by freeform reversible embedding of suspended hydrogels. *Sci Adv*. 2015;1(9):e1500758.

doi: 10.1126/sciadv.1500758

131. Xu T, Jin J, Gregory C, Hickman JJ, Boland T. Inkjet printing of viable mammalian cells. *Biomaterials*. 2005;26(1):93-99.

doi: 10.1016/j.biomaterials.2004.04.011

132. Cui X, Boland T. Human microvasculature fabrication using thermal inkjet printing technology. *Biomaterials*. 2009;30(31):6221-6227.

doi: 10.1016/j.biomaterials.2009.07.056

133. Gao G, Yonezawa T, Hubbell K, Dai G, Cui X. Inkjet-bioprinted acrylated peptides and PEG hydrogel with human mesenchymal stem cells promote robust bone and cartilage formation with minimal printhead clogging. *Biotechnol J*. 2015;10(10):1568-1577.

doi: 10.1002/biot.201400635

134. Gao G, Schilling AF, Yonezawa T, Wang J, Dai G, Cui X. Bioactive nanoparticles stimulate bone tissue formation in bioprinted three-dimensional scaffold and human mesenchymal stem cells. *Biotechnol J*. 2014;9(10):1304-1311.

doi: 10.1002/biot.201400305

135. Shubo X, Xue Y, Xinzhi H, *et al*. Relation between materials, process, structure and property of metallic porous bone scaffolds fabricated by laser powder bed fusion (LPBF): a review. *Opt Laser Technol*. 2025;191:113377.

doi: 10.1016/j.optlastec.2025.113377

136. Yan K, Ngadiman NHA, Saman MZM, Mustafa NS. Advancements in selective laser melting (SLM) of titanium alloy scaffolds for bone tissue engineering. *Biofabrication*. 2025;17(2):022016.

doi: 10.1088/1758-5090/adc6c0

137. Shi Y, Zheng Y, Huang C, *et al*. Influence of Processing Parameters on Additively Manufactured Architected Cellular Metals: Emphasis on Biomedical Applications. *J Funct Biomater*. 2025;16(2):53.

doi: 10.3390/jfb16020053

138. Savov V, Peev S, Yotsova R, Rogova V-V. Influence of SLM-, SLS-, and DMLS-Manufactured Titanium Meshes on Bone Gain Parameters and Complications: A Systematic

Review. *Dent J*. 2025;13(9):387.

doi: 10.3390/dj13090387

139. Alparslan C, Bayraktar Ş. Advances in Digital Light Processing (DLP) Bioprinting: A Review of Biomaterials and Its Applications, Innovations, Challenges, and Future Perspectives. *Polymers (Basel)*. 2025;17(9):1287.

doi: 10.3390/polym17091287

140. Li B, Wang Z, Huang C, *et al*. A comprehensive review on the printing efficiency, precision, and cell viability in 3D bioprinting. *Med Eng Phys*. 2025;145(1):104448.

doi: 10.1016/j.medengphy.2025.104448

141. Corrado F, Di Maio L, Palmero P, *et al*. Vat photo-polymerization 3D printing of gradient scaffolds for osteochondral tissue regeneration. *Acta Biomater*. 2025;200:67-86.

doi: 10.1016/j.actbio.2025.05.042

142. Jing X, Fu H, Yu B, Sun M, Wang L. Two-photon polymerization for 3D biomedical scaffolds: Overview and updates. *Front Bioeng Biotechnol*. 2022;10:994355.

doi: 10.3389/fbioe.2022.994355

143. Fu H, Yu B. 3D micro/nano hydrogel structures fabricated by two-photon polymerization for biomedical applications. *Front Bioeng Biotechnol*. 2024;12:1339450.

doi: 10.3389/fbioe.2024.1339450

144. Nguyen AK, Narayan RJ. Two-photon polymerization for biological applications. *Mater Today*. 2017;20(6):314-322.

doi: 10.1016/j.mattod.2017.06.004

145. O'Halloran S, Pandit A, Heise A, Kellett A. Two-Photon Polymerization: Fundamentals, Materials, and Chemical Modification Strategies. *Adv Sci*. 2022;10(7):2204072.

doi: 10.1002/advs.202204072

146. Binder S, Chalupa-Gantner F, Yoo HW, Zandrini T, Ovsianikov A. Two-photon polymerization system based on a resonant scanner for high-throughput production of tissue engineering microscaffolds. *Addit Manuf*. 2025;97:104601.

doi: 10.1016/j.addma.2024.104601

147. Zein I, Hutmacher DW, Tan KC, Teoh SH. Fused deposition modeling of novel scaffold architectures for tissue engineering applications. *Biomaterials*. 2002;23(4):1169-1185.

doi: 10.1016/s0142-9612(01)00232-0

148. Galea Mifsud M, Di-Silvio L, Coward T. Process-Driven Optimization of FDM Porous PEEK Scaffolds for Alloplastic Bone Grafts. *ACS Omega*. 2025;10(40):47363-47374.

doi: 10.1021/acsomega.5c06631

149. Oberoi G, Nitsch S, Janjić K, *et al*. The impact of 3D-printed LAY-FOMM 40 and LAY-FOMM 60 on L929 cells and human oral fibroblasts. *Clin Oral Investig*. 2021;25(4):1869-1877.

doi: 10.1007/s00784-020-03491-2

150. Gómez-Blanco JC, Galván-Chacón V, Patrocinio D, *et al*. Improving cell viability and velocity in μ-extrusion bioprinting with a novel pre-incubator bioprinter and a standard FDM 3D printing nozzle. *Materials*. 2021;14(11):3100.

doi: 10.3390/ma14113100

151. Sousa HC, Ruben RB, Viana JC. On the Fused Deposition Modelling of Personalised Bio-Scaffolds: Materials, Design, and Manufacturing Aspects. *Bioengineering*. 2024;11(8):769.

doi: 10.3390/bioengineering11080769

152. Zhou G, Liu W, Zhang Y, *et al*. Application of three-dimensional printing in interventional medicine. *J Interv Med*. 2020;3(1):1-16.

doi: 10.1016/j.jimed.2020.01.001

153. Pu X, Wu Y, Liu J, Wu B. 3D bioprinting of microbial-based living materials for advanced energy and environmental applications. *Chem Bio Engineering*. 2024;1(7):568-592.

doi: 10.1021/cbe.4c00024

154. Holland I. Extrusion bioprinting: meeting the promise of human tissue biofabrication? *Prog Biomed Eng*. 2025;7(2):023001.

doi: 10.1088/2516-1091/adb254

155. Li J, Moeinzadeh S, Kim C, *et al*. Development and systematic characterization of GelMA/alginate/PEGDMA/xanthan gum hydrogel bioink system for extrusion bioprinting. *Biomaterials*. 2023;293:121969.

doi: 10.1016/j.biomaterials.2022.121969

156. Wang D, Wang H, Chen X, *et al*. Densification, Tailored Microstructure, and Mechanical Properties of Selective Laser Melted Ti–6Al–4V Alloy via Annealing Heat Treatment. *Micromachines*. 2022;13(2):331.

doi: 10.3390/mi13020331

157. Pasang T, Tavlovich B, Yannay O, *et al*. Directionally-Dependent Mechanical Properties of Ti6Al4V Manufactured by Electron Beam Melting (EBM) and Selective Laser Melting (SLM). *Materials*. 2021;14(13):3603.

doi: 10.3390/ma14133603

158. Zhenhuan W, Yu D, Junsi L, *et al*. Physiochemical and biological evaluation of SLM-manufactured Ti-10Ta-2Nb-2Zr alloy for biomedical implant applications. *Biomed Mater*. 2020;15(4):045017.

doi: 10.1088/1748-605X/ab7ff4

159. Gao X, Ye X, He Y, Ma S, Liu P. Mechanical Properties and Fatigue Life Estimation of Selective-Laser-Manufactured Ti6Al4V Alloys in a Comparison Between Annealing

Treatment and Hot Isostatic Pressing. *Materials*. 2025;18(15):3475.

doi: 10.3390/ma18153475

160. Arif ZU, Khalid MY, Noroozi R, *et al*. Additive manufacturing of sustainable biomaterials for biomedical applications. *Asian J Pharm Sci*. 2023;18(3):100812.

doi: 10.1016/j.ajps.2023.100812

161. Eshraghi S, Das S. Mechanical and microstructural properties of polycaprolactone scaffolds with 1-D, 2-D, and 3-D orthogonally oriented porous architectures produced by selective laser sintering. *Acta Biomater*. 2010;6(7):2467-2476.

doi: 10.1016/j.actbio.2010.02.002

162. Tamaddon M, Samizadeh S, Wang L, Blunn G, Liu C. Intrinsic Osteoinductivity of Porous Titanium Scaffold for Bone Tissue Engineering. *Int J Biomater*. 2017;2017:5093063.

doi: 10.1155/2017/5093063

163. Williams JM, Adewunmi A, Schek RM, *et al*. Bone tissue engineering using polycaprolactone scaffolds fabricated via selective laser sintering. *Biomaterials*. 2005;26(23):4817-4827.

doi: 10.1016/j.biomaterials.2004.11.057

164. Lakkala P, Munnangi SR, Bandari S, Repka M. Additive manufacturing technologies with emphasis on stereolithography 3D printing in pharmaceutical and medical applications: A review. *Int J Pharm X*. 2023;5:100159.

doi: 10.1016/j.ijpx.2023.100159

165. Zandinejad A, Das O, Barmak AB, Kuttolamadom M, Revilla-León M. The Flexural Strength and Flexural Modulus of Stereolithography Additively Manufactured Zirconia with Different Porosities. *J Prosthodont*. 2022;31(5):434-440.

doi: 10.1111/jopr.13430

166. Long T, Tan L, Liu X. Three-dimensional printing in modern orthopedic trauma surgery: a comprehensive analysis of technical evolution and clinical translation. *Front Med*. 2025;12:1560909.

doi: 10.3389/fmed.2025.1560909

167. Ventisette I, Mattii F, Dallari C, *et al*. Gold-Hydrogel Nanocomposites for High-Resolution Laser-Based 3D Printing of Scaffolds with SERS-Sensing Properties. *ACS Appl Bio Mater*. 2024;7(7):4497-4509.

doi: 10.1021/acsabm.4c00379

168. Kim J, Danielak M, Lee DH, *et al*. Advanced dental surgeries using fused filament fabrication and stereolithography printing: Case reports. *Clin Adv Periodontics*. 2026;16(1):132-143.

doi: 10.1002/cap.10344

169. Han Z, Liu S, Qiu K, *et al*. The enhanced ZrO2 produced by DLP via a reliable plasticizer and its dental application. *J Mech Behav Biomed Mater*. 2023;141:105751.

doi: 10.1016/j.jmbbm.2023.105751

170. Shen J, Song W, Liu J, *et al*. 3D bioprinting by reinforced bioink based on photocurable interpenetrating networks for cartilage tissue engineering. *Int J Biol Macromol*. 2024;254:127671.

doi: 10.1016/j.ijbiomac.2023.127671

171. Kornfellner E, Reininger S, Geier S, *et al*. Mechanical properties of additively manufactured lattice structures composed of zirconia and hydroxyapatite ceramics. *J Mech Behav Biomed Mater*. 2024;158:106644.

doi: 10.1016/j.jmbbm.2024.106644

172. Steyrer B, Neubauer P, Liska R, Stampfl J. Visible Light Photoinitiator for 3D-Printing of Tough Methacrylate Resins. *Materials*. 2017;10(12):1445.

doi: 10.3390/ma10121445

173. Huang D, Li Z, Li G, *et al*. Biomimetic structural design in 3D-printed scaffolds for bone tissue engineering. *Mater Today Bio*. 2025;32:101664.

doi: 10.1016/j.mtbio.2025.101664

174. Zhu Y, Gao H, Qiao Q, *et al*. Integrating Additive and Traditional Manufacturing for Multiscale Bone Tissue Engineering Scaffolds. *J Funct Biomater*. 2025;16(9):349.

doi: 10.3390/jfb16090349

175. Laubach M, Herath B, Bock N, *et al*. In vivo characterization of 3D-printed polycaprolactone-hydroxyapatite scaffolds with Voronoi design to advance the concept of scaffold-guided bone regeneration. *Front Bioeng Biotechnol*. 2023;11:1272348.

doi: 10.3389/fbioe.2023.1272348

176. Yun X, Li Z, Yan Z, *et al*. 3D printing combined with thermally induced phase separation for engineering hierarchical osteogenic PLA scaffolds. *Mater Today Bio*. 2025;35:102621.

doi: 10.1016/j.mtbio.2025.102621

177. Hill MJ, Qi B, Bayaniahangar R, *et al*. Nanomaterials for bone tissue regeneration: updates and future perspectives. *Nanomedicine*. 2019;14(22):2987-3006.

doi: 10.2217/nnm-2018-0445

178. Luo Y, Chen B, Zhang X, Huang S, Wa Q. 3D printed concentrated alginate/GelMA hollow-fibers-packed scaffolds with nano apatite coatings for bone tissue engineering. *Int J Biol Macromol*. 2022;202:366-374.

doi: 10.1016/j.ijbiomac.2022.01.096

179. Zhang M, Lin R, Wang X, *et al*. 3D printing of Haversian bone–mimicking scaffolds for multicellular delivery in bone regeneration. *Sci Adv*. 2020;6(12):eaaz6725.

doi: 10.1126/sciadv.aaz6725

180. Xu C, Ivanovski S. Clinical translation of personalized bioengineered implant scaffolds. *Nat Rev Bioeng*. 2025;3(5):390-407.

doi: 10.1038/s44222-024-00269-z

181. Zhang B, Wang L, Song P, *et al*. 3D printed bone tissue regenerative PLA/HA scaffolds with comprehensive performance optimizations. *Mater Des*. 2021;201:109490.

doi: 10.1016/j.matdes.2021.109490

182. Tu C, Chen J, Huang C, *et al*. Effects of electromagnetic fields treatment on rat critical-sized calvarial defects with a 3D-printed composite scaffold. *Stem Cell Res Ther*. 2020;11(1):433.

doi: 10.1186/s13287-020-01954-7

183. Ebel F, Schön S, Sharma N, *et al*. Clinical and patient-reported outcome after patient-specific 3D printer-assisted cranioplasty. *Neurosurg Rev*. 2023;46(1):93.

doi: 10.1007/s10143-023-02000-9

184. da Silva Júnior EB, de Aragão AH, de Paula Loureiro M, *et al*. Cranioplasty with three-dimensional customised mould for polymethylmethacrylate implant: a series of 16 consecutive patients with cost-effectiveness consideration. *3D Print Med*. 2021;7(1):4.

doi: 10.1186/s41205-021-00096-7

185. Herath B, Laubach M, Suresh S, *et al*. Modular design workflow for 3D printable bioresorbable patient-specific bone scaffolds: extended features and clinical validation. *Front Bioeng Biotechnol*. 2024;12:1404481.

doi: 10.3389/fbioe.2024.1404481

186. Liang H, Chen B, Duan S, *et al*. Treatment of complex limb fractures with 3D printing technology combined with personalized plates: a retrospective study of case series and literature review. *Front Surg*. 2024;11:1383401.

doi: 10.3389/fsurg.2024.1383401

187. Zheng P, Yao Q, Mao F, *et al*. Adhesion, proliferation and osteogenic differentiation of mesenchymal stem cells in 3D printed poly-ε-caprolactone/hydroxyapatite scaffolds combined with bone marrow clots. *Mol Med Rep*. 2017;16(4):5078-5084.

doi: 10.3892/mmr.2017.7266

188. Lin Z, Wu M, He H, *et al*. 3D printing of mechanically stable calcium-free alginate-based scaffolds with tunable surface charge to enable cell adhesion and facile biofunctionalization. *Adv Funct Mater*. 2019;29(9):1808439.

doi: 10.1002/adfm.201808439

189. Yan Y, Chen H, Zhang H, *et al*. Vascularized 3D printed scaffolds for promoting bone regeneration. *Biomaterials*. 2019;190-191:97-110.

doi: 10.1016/j.biomaterials.2018.10.033

190. Zhu C, Pongkitwitoon S, Qiu J, Thomopoulos S, Xia Y. Design and Fabrication of a Hierarchically Structured Scaffold for Tendon-to-Bone Repair. *Adv Mater*. 2018;30(16):e1707306.

doi: 10.1002/adma.201707306

191. Nguyen LH, Annabi N, Nikkhah M, *et al*. Vascularized Bone Tissue Engineering: Approaches for Potential Improvement. *Tissue Eng Part B Rev*. 2012;18(5):363-382.

doi: 10.1089/ten.TEB.2012.0012

192. Boudene I, Bougdid Y. Two-photon polymerization-assisted 3D laser nanoprinting: from fundamentals to modern applications. *J Mater Chem C*. 2025;13(36):18597-18630.

doi: 10.1039/d5tc02037a

193. Basu P. Advancements in Two-Photon Polymerization (2PP) for Micro and Nanoscale Fabrication. *Nanomanufacturing*. 2026;6(1):1.

doi: 10.3390/nanomanufacturing6010001

194. Snow F, Doyle SE, Liu E, *et al*. A detailed guide to melt electrowriting for tissue engineering applications. *Biofabrication*. 2025;17(4):042004.

doi: 10.1088/1758-5090/adfbc4

195. Yin Y, Yang H, Han W, *et al*. Melt Electrowriting for Biomimetic Tissue Engineering: Advances in Scaffold Design, Materials, and Multifunctional Applications. *Polym Adv Technol*. 2025;36(1):e70067.

doi: 10.1002/pat.70067

196. Hu Z, Lin H, Wang Z, *et al*. 3D Printing Hierarchical Porous Nanofibrous Scaffold for Bone Regeneration. *Small*. 2025;21(2):2405406.

doi: 10.1002/smll.202405406

197. Liu B, Li J, Lei X, *et al*. 3D-bioprinted functional and biomimetic hydrogel scaffolds incorporated with nanosilicates to promote bone healing in rat calvarial defect model. *Mater Sci Eng C Mater Biol Appl*. 2020;112:110905.

doi: 10.1016/j.msec.2020.110905

198. Codrea CI, Baykara D, Mitran R-A, Koyuncu ACÇ, Gunduz O, Ficai A. 3D-bioprinted gelatin methacryloyl-strontium-doped hydroxyapatite composite hydrogels scaffolds for bone tissue regeneration. *Polymers (Basel)*. 2024;16(13):1932.

doi: 10.3390/polym16131932

199. Allen NB, Abar B, Johnson L, Burbano J, Danilkowicz RM, Adams SB. 3D-bioprinted GelMA-gelatin-hydroxyapatite osteoblast-laden composite hydrogels for bone tissue engineering. *Bioprinting*. 2022;26:e00196.

doi: 10.1016/j.bprint.2022.e00196

200. Miao S, Zhou J, Liu B, *et al*. A 3D bioprinted nano-laponite hydrogel construct promotes osteogenesis by activating PI3K/AKT signaling pathway. *Mater Today Bio*.

2022;16:100342.

doi: 10.1016/j.mtbio.2022.100342

201. Lee SS, Du X, Kim I, Ferguson SJ. Scaffolds for bone-tissue engineering. *Matter*. 2022;5(9):2722-2759.

doi: 10.1016/j.matt.2022.06.003

202. Li Q, Nikolova MT, Zhang G, *et al*. Macro-scale, scaffold-assisted model of the human bone marrow endosteal niche using hiPSC-vascularized osteoblastic organoids. *Cell Stem Cell*. 2025;32(12):1941-1958.e8.

doi: 10.1016/j.stem.2025.10.009

203. Chen J, Liang R, Jia S, *et al*. Spatiotemporal Adaptation in 4D Bioprinting for Dynamic Bone and Cartilage Regeneration. *Adv Funct Mater*. 2026;36(28):e22357.

doi: 10.1002/adfm.202522357

204. Zarei A, Farazin A. Synergizing additive manufacturing and machine learning for advanced hydroxyapatite scaffold design in bone regeneration. *J Aust Ceram Soc*. 2025;61(3):797-813.

doi: 10.1007/s41779-024-01084-w